

BLACK HOLES IN PSEUDOBULGES AND SPHEROIDALS: A CHANGE IN THE BLACK HOLE-BULGE SCALING RELATIONS AT LOW MASS<sup>1</sup>JENNY E. GREENE<sup>2</sup>

Department of Astrophysical Sciences, Princeton University, Princeton, NJ

LUIS C. HO

The Observatories of the Carnegie Institution of Washington, 813 Santa Barbara St., Pasadena, CA 91101

AARON J. BARTH

Department of Physics and Astronomy, University of California at Irvine, 4129 Frederick Reines Hall, Irvine, CA 92697

*To appear in The Astrophysical Journal.*

## ABSTRACT

We investigate the relationship between black hole mass and host galaxy properties for active galaxies with the lowest black hole masses currently known in galaxy nuclei. *Hubble Space Telescope* imaging confirms that the host galaxies have correspondingly low luminosity; they are  $\sim 1$  mag below  $L^*$ . In terms of morphology,  $\sim 60\%$  of the sample are disk-dominated, and all of these are consistent with containing a bulge or (more likely) pseudobulge, while the remainder are compact systems with no discernible disk component. In general the compact components of the galaxies do not obey the fundamental plane of giant elliptical galaxies and classical bulges, but rather are less centrally concentrated at a given luminosity, much like spheroidal galaxies. Our results strongly confirm that a classical bulge is not a requirement for a nuclear black hole. At the same time, the observed ratio of black hole to bulge mass is nearly an order of magnitude lower in this sample than that seen for classical bulges. While the  $M_{\text{BH}} - \sigma_*$  relation appears to continue to low mass, it seems that black hole-galaxy scaling relations do depend on galaxy structure.

*Subject headings:* galaxies: active — galaxies: nuclei — galaxies: Seyfert

## 1. INTRODUCTION

The discovery of a tight correlation of supermassive black hole (BH) mass with the properties of the elliptical galaxies and classical bulges in which they are found (e.g., the  $M_{\text{BH}} - \sigma_*$  relation; Tremaine et al. 2002) suggests that there is an underlying tight correspondence between the growth of the two galaxy components. Furthermore, the extremely regular structural properties of elliptical galaxies and spiral bulges (the fundamental plane; Dressler et al. 1987; Djorgovski & Davis 1987) imply very similar formation paths for the two populations; apparently one aspect of that formation involves the growth of a supermassive BH. For instance, if elliptical galaxies grow through hierarchical merging, perhaps BH accretion episodes are instigated during violent merging (e.g., Hopkins et al. 2006), and this accretion self-regulates the growth of the BH according to the depth of the galaxy potential well, thus leading to the  $M_{\text{BH}} - \sigma_*$  relation (e.g., Silk & Rees 1998). In principle, a useful test of the BH-bulge connection is to look at the masses of BHs in galaxies that have not developed classical bulges, to see whether the BH masses in these galaxies have a similar or different relation to their surrounding hosts.

Due to technical challenges, BH demographics in late-type galaxies are virtually unconstrained. Low-mass BHs are difficult to weigh because they have a very small gravitational sphere of influence. The only late-type galaxies with stellar-dynamical constraints on the presence of nuclear BHs are within the Local Group; the late-type spiral galaxy M33 (Gebhardt et al. 2001) and the spheroidal galaxy NGC 205 (Valluri et al. 2005) have upper limits on their BH masses significantly below expectations based on the  $M_{\text{BH}} - \sigma_*$  relation. This is not

necessarily surprising; if BH growth is associated with bulge formation, then perhaps we should not expect to find BHs in galaxies with little or no bulges, or whose bulgelike central concentration formed through very different mechanisms than did classical bulges. Furthermore, low-mass galaxies may have trouble retaining their BHs. The anisotropic gravitational radiation associated with an unequal-mass BH merger event can impart a net velocity to the BH remnant that exceeds the escape velocity of a dwarf galaxy (e.g., Merritt et al. 2004; Volonteri 2007). All theoretical suppositions aside, better observational constraints are needed on the occupation fraction of BHs in low-mass galaxies. Without the luxury of dynamical constraints, we are forced to use indirect tracers, in the form of nuclear activity, to constrain the presence or absence of BHs in low-mass galaxies.

There are two well-studied low-mass galaxies with active nuclei. NGC 4395 is an Sdm spiral galaxy only 4 Mpc away (Filippenko & Sargent 1988; Filippenko & Ho 2003) while POX 52 (Kunth et al. 1987) is a spheroidal galaxy whose nature has been recently revisited based on updated measurements (Barth et al. 2004; Thornton et al. 2008). Both of these galaxies and the globular cluster G1 (Gebhardt et al. 2002, 2005; Ulvestad et al. 2007) appear to obey the low-mass extrapolation of the  $M_{\text{BH}} - \sigma_*$  relation. This intriguing fact inspired Greene & Ho (2004, 2007c) to search systematically for BHs with masses  $< 10^6 M_\odot$  using the Sloan Digital Sky Survey (York et al. 2000). Follow-up spectroscopy revealed that, like their nearby counterparts, they also obey the low-mass extrapolation of the  $M_{\text{BH}} - \sigma_*$  relation (Barth et al. 2005). However, the physical significance of  $\sigma_*$  for these systems is not immediately clear in

<sup>1</sup>Based on observations made with the NASA/ESA Hubble Space Telescope, obtained at the Space Telescope Science Institute, which is operated by the Association of Universities for Research in Astronomy, Inc., under NASA contract NAS 5-26555. These observations are associated with program GO-10596.

<sup>2</sup>Hubble, Princeton-Carnegie Fellow

the absence of more detailed host galaxy structural information. In this work we use *Hubble Space Telescope* (HST) Advanced Camera for Surveys (ACS) imaging to constrain the structural properties of the host galaxies of the 19 low-mass BHs from Greene & Ho (2004).

One of the particularly appealing aspects of this sample is that in addition to low mass, the objects are radiating at high fractions of their Eddington limit. We thus have the opportunity to perform a detailed study of the host galaxy environments of BHs that are experiencing a significant growth episode, which is impossible for more massive BHs that are no longer actively accreting locally (e.g., Heckman et al. 2004; Greene & Ho 2007b). A number of suggestions have been made that low-mass, high-Eddington ratio AGNs have anomalously low BH masses compared to their surrounding galaxies, based both on the linewidths of the narrow emission lines (e.g., Bian & Zhao 2004; Grupe & Mathur 2004), and the circular velocity of the host inferred from the integrated H I linewidth (Ho et al. 2008). Although the Greene & Ho systems appear to obey the low-mass extrapolation of the  $M_{\text{BH}} - \sigma_*$  relation (Barth et al. 2005), it will be very instructive to examine the host galaxy luminosity and structure as well.

A brief explanation is in order regarding our use of terminology. A principal goal of the study is to use the locations of our AGN host galaxies on the fundamental plane to infer the nature and formation histories of these galaxies. We therefore wish to be very careful that our naming conventions reflect what we believe are physically meaningful distinctions between different classes of objects. Elliptical galaxies and the classical bulges that are found in the centers of early-type disk galaxies both obey the fundamental plane (e.g., Bender et al. 1992). However, not all bulge components appear to be built like small elliptical galaxies. Particularly in late-type spirals, bulge components increasingly depart from the structural and stellar population properties that define elliptical galaxies and begin to look more like disks. These so-called pseudobulges are characterized by a high degree of rotational support, exponential profiles, ongoing star formation or starbursts, and nuclear bars or spirals (see review in Kormendy & Kennicutt 2004). In general, the properties of pseudobulges suggest that they have formed through dissipative processes and have evolved secularly, over many disk rotation periods.

At even lower galaxy mass, there is yet another sequence of stellar systems, of which NGC 205 is a local example. These objects are small-scale, hot stellar systems, and thus are often called “dwarf elliptical galaxies”. However, based on their structural properties (specifically, their position in the fundamental plane) they are nothing like small elliptical galaxies. There are real elliptical galaxies at these luminosities, such as M32. In contrast, spheroidal galaxies, as we will call them, are clearly less centrally concentrated than elliptical galaxies at the same luminosity (e.g., Wirth & Gallagher 1984; Kormendy 1985). The alternate view, that elliptical and spheroidal galaxies form a continuous sequence, has been expressed in the literature, based predominantly on the continuity in the sequence of surface brightness profile shapes as a function of luminosity between the two sequences (e.g., Jerjen & Binggeli 1997; Graham & Guzmán 2003; Ferrarese et al. 2006). In our view the controversy has been definitively settled by the comprehensive photometric study of Kormendy et al. (2008; see also e.g., Geha et al. 2002), which demonstrates that elliptical and spheroidal galaxies are cleanly separated in the fundamental plane projec-

tions, even in the region of luminosity overlap between these two classes of galaxies. The implication of this distinction is of critical importance in the context of our study; it suggests that spheroidal galaxies do not share the violent merger history of elliptical galaxies, but rather formed in a manner similar to disk galaxies (e.g., Kormendy 1985; Bender et al. 1992). In this interpretation, spheroidals and pseudobulges presumably have more in common than spheroidal and elliptical galaxies. We are in a position to evaluate (a) whether there is a population of galaxies without classical bulges that nevertheless host central BHs and (b) how the relationship between BH mass and “bulge” mass depends on the host galaxy structure. In this paper we follow Kormendy et al. (2008) and explicitly use the term “spheroidals” to describe systems that in the literature are often called “dwarf ellipticals”.

Throughout we assume the following cosmological parameters to calculate distances:  $H_0 = 100 h = 71 \text{ km s}^{-1} \text{ Mpc}^{-1}$ ,  $\Omega_m = 0.27$ , and  $\Omega_\Lambda = 0.75$  (Spergel et al. 2003).

## 2. THE SAMPLE

Our intermediate-mass BHs are selected from the SDSS sample of AGNs with broad H $\alpha$  ( $z < 0.352$ ), described in detail in Greene & Ho (2004). Throughout we will refer to the targets using the identification numbers assigned in that paper. The 19 AGNs in this sample have been followed up extensively in the radio (Greene et al. 2006), X-ray (Greene & Ho 2007a; Miniutti et al. 2008), and mid-infrared with *Spitzer*. Furthermore, most have stellar velocity dispersions measurements taken with ESI on Keck (Barth et al. 2005). The sample is selected to have BH masses  $M_{\text{BH}} < 10^6 M_\odot$  and to have minimal galaxy continuum within the SDSS aperture. One of the primary goals of our original search was to investigate the host galaxy properties of a BH mass-selected sample of low-mass BHs. We pursue that goal here.

It is worth noting, however, that there are implicit constraints on the host galaxy light set by the selection process, which are discussed in detail by Greene & Ho (2007b). To be spectroscopically targeted by the SDSS the galaxy must be relatively bright, while to be spectroscopically identified as a broad-line AGN based on the H $\alpha$  profile the host galaxy must not swamp the weak emission lines. When we model these constraints, we find a range of possible host galaxy luminosities that is very similar to that of the observed distribution. Although our search was designed to be free of host galaxy bias, in fact there is a strong implicit host galaxy luminosity bias built into our selection process, which must be considered when interpreting our results. Nevertheless, despite this major caveat, it is still of considerable interest to examine the host galaxy properties of this unique sample.

Since the sample selection is based on BH mass, we must also discuss our BH mass measurement technique. Of course, dynamical techniques that use the motions of stars or gas in the vicinity of the BH (e.g., Gebhardt et al. 2000a) provide the most accurate BH mass measurements. However, as discussed above, the spatial resolution requirements are beyond current capabilities, and thus we are forced to rely on less direct mass indicators. In this case the dense gas orbiting the BH (the broad-line region or BLR) is assumed to be virialized and is used as a dynamical tracer. The BLR velocity dispersion is derived from the width of a broad line (in our case H $\alpha$ ; Greene & Ho 2005b). BLR sizes have been measured for a handful of nearby AGNs by measuring the lag between variability in the AGN continuum and corresponding variability in the line emission (rever-

beration mapping; Blandford & McKee 1982; Peterson et al. 2004). With measured BLR radii, it is possible to calibrate an empirical relation between the AGN luminosity and the BLR size (e.g., Kaspi et al. 2005; Bentz et al. 2006), and from this relation to estimate BH masses from single-epoch spectroscopy. We will refer to masses measured in this manner as “virial” BH masses.

A host of potentially very serious systematic uncertainties are inherent in this technique (e.g., Krolik 2001; Collin et al. 2006), particularly since the AGNs in our sample are considerably less luminous, and harbor less massive BHs, than the bulk of the reverberation mapping sample. Nevertheless, in the cases for which they are available,  $\sigma_*$  measurements show reassuring agreement with both reverberation-mapping masses (Gebhardt et al. 2000b; Ferrarese et al. 2001; Onken et al. 2004; Nelson et al. 2004) and the virial masses of significantly larger samples of AGNs (Greene & Ho 2006b; Shen et al. 2008a).

Finally, the technical measurement details can seriously and systematically impact the derived BH masses (e.g., Collin et al. 2006; Shen et al. 2008b). Note, for instance, that the BH masses presented herein differ from those in the original Greene & Ho (2004) paper (and in some cases are greater than the original mass limit of  $10^6 M_\odot$ ), both because of differences in line width measurements between the SDSS and ESI spectra (Barth et al. 2005) and because of revision to the relation between BLR radius and AGN luminosity (Bentz et al. 2006). In this paper, we will use the  $H\alpha$  calibration of Greene & Ho (2005b), and the most recent calibration of the radius-luminosity relation presented by Bentz et al. (2006). We explain our measurement procedure in detail in the Appendix of Greene & Ho (2007c), and the interested reader is directed there for more information.

### 3. OBSERVATIONS AND METHODS

We were awarded 19 orbits in Cycle 14 to observe the 19 Greene & Ho (2004) targets with *HST*/ACS. The observation dates and durations are shown for each target in Table 1; GH03 is excluded due to a guide-star acquisition failure and will not be discussed further. Each orbit was equally divided between F814W (broad *I* band) and F435W (*B* band), but due to saturation concerns, the F814W observation was split between a short (30 s) and long ( $\sim 900$  s) exposure. Although the *HST* and Johnson filters are not identical, for convenience we refer to F435W as *B* and F814W as *I* throughout the manuscript<sup>4</sup>. Both for cosmic ray removal and improvement of the final image sampling, the images were taken in two dither steps, using a standard ACS two-step dither pattern. The *I*-band images are the main focus of this paper; because of the high throughput and red color of this wide filter, it is optimal for probing host galaxy structure. On the other hand, the *B*-band images provide important constraints on the presence and morphology of ongoing star formation. Furthermore, because the AGNs are blue, we are able to derive our most robust measurements of the AGN luminosity from these images, which leads to a significant improvement in our estimate of the BH mass.

Data reduction (bias subtraction and flat-fielding) was performed by the ACS CALACS software pipeline (Pavlovsky et al. 2005). The dithered images are combined and cleaned of cosmic rays using the MULTIDRIZZLE software (Koekemoer et al. 2002), which linearly reconstructs the image, accounting

for geometric distortion (Fruchter & Hook 2002). We make only minor changes to the default parameters. One is to perform our own cosmic ray rejection using software written by P. Martini. The other is to keep the native orientation of the images (as opposed to specifying North up in the final images). This latter step is necessary to ensure that the stars we use as models of the point-spread function (PSF) are oriented properly across all images. No sky subtraction is performed at this stage. The resultant images have a resolution of  $\text{FWHM}=0''.11$ , as measured from bright stars in the *I*-band images, and a corresponding typical physical resolution of  $\sim 170$  pc at the median  $z \approx 0.08$ . We reach a typical  $10\sigma$  limiting surface brightness of  $23.7 \text{ mag arcsec}^{-2}$  in the *I* band. All magnitudes are reported in the Vega system.

#### 3.1. The Point-Spread Function

One of the major benefits of *HST* is, of course, the very stable PSF. However, even in the absence of atmosphere, the *HST*/ACS PSF is known to vary as a function of both detector position and time (e.g., Sirianni et al. 2005; Rhodes et al. 2007). Note that for our application the PSF shape is of particular importance due to the presence of a strong nuclear point source. For the *I* filter, we have reconstructed PSF models from three bright stars in the fields of GH02, GH16, and GH17, respectively. The stars are significantly brighter than any of the AGNs; they are saturated in the long exposure, but luckily we have a measurement of the core from the 30 s image. These PSF stars were observed at different times (between Oct. and Nov. of 2005) and are at different positions ( $\sim 300, 800$ , and  $600$  pixels from the typical object position, respectively). We also use the TinyTim software (Krist 1995), which models both the spatial and spectral variations in the PSF, and accounts for effects such as charge diffusion that tend to broaden the PSF. While it would be ideal to have a PSF star observation for each object, we can at least quantify the systematic uncertainty arising from PSF mismatch as the differences between fits using each PSF star. For the F435W filter, we rely exclusively on TinyTim models and an IDL wrapper (Rhodes et al. 2006, 2007) that further generates PSF models with focus values of  $\pm 5\mu\text{m}$  around the nominal focus, to use the terminology of Rhodes et al.

#### 3.2. Non-parametric Magnitudes

Perhaps the most basic measurement we might make is that of the total host galaxy and AGN luminosity in each band. For this purpose we need not assume any model for the host galaxy light; we need only a model of the PSF. Prior to performing detailed fits to the two-dimensional image profiles, we perform non-parametric measurements of the AGN and host galaxy magnitudes.

The basic premise in deriving non-parametric magnitudes is that within a small enough aperture at the center of the galaxy, the AGN completely dominates the luminosity. Thus one simply scales the model PSF to match the AGN flux within this small aperture, and subtracts the scaled PSF magnitude. To the extent that the PSF model is an accurate representation of the light distribution of the AGN, aperture effects are automatically accounted for. This method fails systematically, however, when the AGN does not dominate the light within the chosen

<sup>4</sup> We often compare our results to fiducial colors of galaxies as a function of Hubble type using the synthetic photometry of Fukugita et al. (1995). Although that photometry was performed in the Johnson *B* and *I* filters, the differences between these and the *HST* filters are  $< 0.05$  mag for all spectral types (as we verified using *synphot* in IRAF). Since intrinsic variations in color due to reddening and stellar populations are always larger than this, we do not worry further about the filter differences.

Table 1. Sample and Observations

Name (1)	SDSS Name (2)	$D_L$ (3)	$A_B$ (4)	Obs. Date (5)	$t^B$ (6)	$t^I$ (7)	$\log \lambda L_{5100\text{\AA}}$ (8)	FWHM $_{H\alpha}$ (9)	$\log M_{BH}$ (10)	$\sigma_*$ (11)
GH01	SDSS J010712.03+140844.9	343	0.30	2005-09-06	1100	917	42.43 $\pm$ 0.10	950	5.9	36 $\pm$ 6
GH02	SDSS J024912.86-081525.6	127	0.13	2005-10-13	1092	916	41.34 $\pm$ 0.14	690	5.1	50 $\pm$ 4
GH04	SDSS J082912.67+500652.3	189	0.18	2005-10-23	1188	1031	41.85 $\pm$ 0.12	760	5.4	60 $\pm$ 4
GH05	SDSS J094310.12+604559.1	331	0.11	2006-02-02	1236	1061	42.49 $\pm$ 0.04	720	5.7	...
GH06	SDSS J101108.40+002908.7	455	0.15	2005-11-03	1090	912	42.17 $\pm$ 0.03	1240	6.0	48 $\pm$ 7
GH07	SDSS J101627.32-000714.5	427	0.15	2005-11-04	1090	912	42.35 $\pm$ 0.06	1140	6.0	39 $\pm$ 6
GH08	SDSS J114008.71+030711.4	364	0.09	2005-12-25	1090	912	42.77 $\pm$ 0.04	800	5.9	...
GH09	SDSS J115138.24+004946.4	939	0.11	2005-12-24	1090	912	42.79 $\pm$ 0.04	810	6.0	...
GH10	SDSS J124035.81-002919.4	363	0.11	2006-02-21	1090	912	42.57 $\pm$ 0.04	720	5.7	49 $\pm$ 7
GH11	SDSS J125055.28-015556.6	365	0.10	2005-12-22	1090	912	41.78 $\pm$ 1.22	2110	6.3	64 $\pm$ 6
GH12	SDSS J135724.52+652505.8	484	0.09	2005-12-06	1278	1102	42.85 $\pm$ 0.02	880	6.1	...
GH13	SDSS J141234.67-003500.0	584	0.20	2006-02-17	1090	912	42.89 $\pm$ 0.06	980	6.2	...
GH14	SDSS J143450.62+033842.5	121	0.17	2006-04-02	1090	912	40.92 $\pm$ 0.93	770	4.9	48 $\pm$ 7
GH15	SDSS J144507.30+593649.9	589	0.03	2005-09-29	1230	1053	42.58 $\pm$ 0.05	1230	6.2	...
GH16	SDSS J170246.09+602818.9	307	0.08	2005-11-10	1236	1061	42.27 $\pm$ 0.07	1170	6.0	69 $\pm$ 6
GH17	SDSS J172759.15+542147.0	452	0.17	2005-11-14	1198	1021	42.58 $\pm$ 0.02	930	6.0	58 $\pm$ 7
GH18	SDSS J232159.06+000738.8	880	0.19	2006-05-13	1090	912	42.64 $\pm$ 0.06	1770	6.6	81 $\pm$ 9
GH19	SDSS J233837.10-002810.3	154	0.13	2006-05-17	1090	890	41.06 $\pm$ 0.19	1890	5.8	58 $\pm$ 4

Note. — Col. (1): Object name from Greene & Ho 2004. Col. (2): Official SDSS name. Col. (3): Luminosity distance (Mpc). Col. (4): Galactic reddening in the  $B$  band (mag). Col. (5): Date of *HST* observation. Col. (6): Total duration of F435W exposure (sec). Col. (7): Total duration of F814W long exposure (sec; not including a 30 sec exposure in case of saturation.) Col. (8): AGN continuum luminosity at 5100 Å (ergs s $^{-1}$ ), as measured from the GALFIT models to the  $B$ -band images. Col. (9):  $H\alpha$  linewidth (km s $^{-1}$ ) taken from Barth et al. 2005 when available and Greene & Ho 2007b in all other cases. Col. (10): Virial  $M_{BH}$  ( $M_\odot$ ) using  $L_{5100\text{\AA}}$  from Col. (8), FWHM from Col. (9), the Bentz et al. 2006 radius-luminosity relation, and assuming  $f = 0.75$ . Col. (11): Stellar velocity dispersion (km s $^{-1}$ ) from Barth et al. 2005.

aperture. It is desirable to choose the smallest possible aperture to mitigate contamination from the host galaxy, in principle as small as a single pixel. Unfortunately, using a single pixel makes the procedure very sensitive to centering errors. For that reason, we follow Jahnke et al. (2004) and measure the unresolved nuclear magnitude within an aperture of radius 2 pixels. We perform the photometry using the package *phot* within IRAF and apertures of 1–200 pixels in radius. The sky is subtracted from each aperture as determined from an aperture of radius 220 pixels and a width of 20 pixels. Again, of primary concern is the systematic overestimate of the AGN luminosity that necessarily ensues due to our assumption that it accounts for 100% of the light within the inner pixels. The appropriateness of this assumption depends on both the contrast between the AGN and the host galaxy, and the light distribution of the host galaxy. Centrally concentrated hosts are the most difficult to uncover.

The outer apertures are incremented in five-pixel steps until the magnitude is stable to within 0.05 mag. These non-parametric magnitudes, both for the AGN and the total galaxy luminosity are presented in Table 2. It is clear from this exercise that, as claimed in Greene & Ho (2004), the host galaxies are generally much brighter than the AGNs, unlike luminous AGNs, whose host galaxies may account for only  $\sim 10\%$  of the total luminosity of the system. Even using the non-parametric PSF-scaled luminosities, which may be viewed as an upper limit on the total nuclear strength, we find that on average the AGN accounts for only 30% of the total luminosity in the  $B$  band and 20% of the total luminosity in the  $I$  band. Only in GH15 does the nuclear luminosity exceed the galaxy luminos-

ity. Therefore, in the majority of cases we should be able to measure robust galaxy structural parameters for these galaxies. We compare the results of the parametric and non-parametric photometry below, and find reassuringly good agreement.

### 3.3. GALFIT

Non-parametric measurements provide a valuable benchmark for our subsequent work since they are model-independent. Still, we wish to parametrize the structures of our host galaxies, for comparison with inactive local galaxies. Furthermore, since all fit parameters are coupled, without a model for the inner galaxy profile it is not possible to get a proper measurement of the AGN magnitude. For this reason, we proceed now to parametrized fitting.

Generally speaking, our goal is to decompose the observed intensity distribution into a combination of components including a central unresolved point source, and some combination of a possible disk, bulge, and bar. In general profile-fitting can be performed either with azimuthally averaged profiles or full two-dimensional images. Fitting the full two-dimensional profile can provide important additional constraints (for instance in the presence of ellipticity changes with radius), and in the presence of multiple complex components (such as nuclei and bars) this flexibility is of particular importance (e.g., Andredakis et al. 1995; Byun & Freeman 1995, Wadadekar et al. 1999). Here we utilize the versatile GALFIT routine to perform two-dimensional profile decompositions (Peng et al. 2002). GALFIT has been used and tested extensively for a variety of applications including AGN host-galaxy work (e.g., Ho & Peng 2001; Peng et al. 2006a, 2006b; Kim et al. 2007), and galaxy

morphology work at low (e.g., Peng 2002) and high (e.g., Bell et al. 2006) redshift.

Briefly, the current version of GALFIT models each galaxy component as an azimuthally symmetric ellipsoid, with a number of possible radial intensity profiles, including the generalized Sérsic (1968) model

$$I(r) = I_e \exp \left[ -b_n \left( \frac{r}{r_e} \right)^{1/n} - 1 \right], \quad (1)$$

where  $r_e$  is the effective (half-light) radius,  $I_e$  is the intensity at  $r_e$ ,  $n$  is the Sérsic index, and  $b_n$  is chosen such that

$$\int_0^\infty I(r) 2\pi r dr = 2 \int_0^{r_e} I(r) 2\pi r dr. \quad (2)$$

We adopt the analytic approximation for  $b_n$  from MacArthur et al. (2003), as adapted from Ciotti & Bertin (1999):

$$b_n \approx 2n - \frac{1}{3} + \frac{4}{405n} + \frac{46}{25515n^2} + \frac{131}{1148175n^3} - \frac{2194697}{30690717750n^4}. \quad (3)$$

The Sérsic model is particularly convenient, as it reduces to an exponential profile for  $n = 1$  and a de Vaucouleurs (1948) profile for  $n = 4$ . Bars may be modeled as ellipsoids with very low axial ratios. We follow de Jong (1996a; see also Freeman 1966) and model the intensity distribution in the bar as a Gaussian ( $n = 0.5$ ). In total for a given Sérsic component, the model parameters include the two-dimensional component centroid, the total magnitude, the Sérsic index, the effective radius, the position angle, and the ellipticity (which are constants with radius for a given component in this version of GALFIT). Parameter estimation is performed using Levenberg-Marquardt minimization of  $\chi^2$  in pixel space. The sky is modeled as a constant pedestal offset. The effects of the telescope optics are accounted for by convolution with a user-provided model of the instrumental PSF, and foreground objects or detector gaps are explicitly masked with a user-defined bad-pixel list. In general, for the single-component models predominantly discussed here, GALFIT is able to converge rapidly with only moderately reasonable input parameters.

Frequently the *HST* PSF is actually undersampled. The problem is most severe for WFPC2, but even ACS/WFC, with  $0''.05$  pixels, is undersampled. As a result, centering mismatch occurs at a level that leads to significant parameter estimation errors. M. Kim et al. (in preparation) use simulations to show that significant systematic uncertainty can result from the impact of undersampling. They recommend broadening the image and PSF with a  $\sigma = 2$  pixel Gaussian kernel, which they show largely mitigates the systematic offsets in their simulations. Therefore, we also perform the fitting with a broadened PSF star, using the stars from the GH02 and GH16 observations, which tend to provide the best fits.

In what follows, we discuss the structural properties of the host galaxies as derived from GALFIT models of the *I*-band images, since the host galaxy contrast is maximized in this band. The AGN is modeled as a scaled version of the PSF, while the host galaxies are modeled as Sérsic components. We have performed fits to the *B*-band images as well, in which all of the structural measurements are fixed to the *I*-band fits, but the magnitudes are allowed to vary. The *B*-band fits, while shallow, provide our most robust measurement of the AGN luminosity. We do not have a strong handle on the intrinsic reddening nor on the true galaxy color, and so we do not assume a particular value for the reddening.

## 4. RESULTS

Even in the absence of a bright nuclear point source, profile decomposition is a difficult endeavor, and without sufficient depth and angular resolution parameter coupling renders the extraction of multiple components unreliable (e.g., Kormendy & Djorgovski 1989; MacArthur et al. 2003). The active nucleus only accentuates these difficulties. Therefore, while GALFIT in principle can solve for any number of completely general Sérsic components, we are forced to consider a much more restricted set of models. First, we divide the sample into those systems with a clear disk component<sup>5</sup> (GH01, GH02, GH05, GH06, GH08, GH13, GH14, GH15, GH18, GH19), and those that are simply “blobs” (we agnostically refer to compact, smooth galaxies as blobs, since until we examine their structures in detail we do not know whether they are elliptical or spheroidal galaxies; see Fig. 1). We fit the profile with a minimum number of components, and then place limits on the existence of a second component (disk or bulge for the blob or disk galaxies, respectively). We make the further assumption that the underlying galaxies obey structural scaling relations akin to inactive systems, and use these scalings to limit parameter space when deriving limits. Since the details are different for the blob and disk systems, we discuss each subsample separately below.

### 4.1. Blobs

Particularly in the case of steep Sérsic profiles, a nuclear point source complicates our ability to recover the true index  $n$ . For this reason, rather than allowing the Sérsic index to float, we simply run a grid of models with  $n = 1, 2, 3, 4$ , and then ask which does the best job at fitting the data. The  $\chi^2$  values returned by GALFIT, while they have some relative value, do not have any absolute discriminatory power, because we are dominated by systematic uncertainties (§4.3). To assist in determining the best-fit Sérsic index, we also compute a  $\chi^2$  from radial profiles of both the best-fit model and the data constructed using the program *ellipse* within IRAF, which is based on the techniques described in Jedrzejewski (1987). We report best-fit values averaged over all PSF stars, and we include in the error budget the range of luminosities and sizes that ensues from a range in Sérsic index of  $n \pm 1$ . While we might expect these low-luminosity galaxies to have relatively low Sérsic indices based on the correlation between galaxy luminosity and Sérsic index (e.g., Schombert 1986; Caon et al. 1993; Graham et al. 1996; MacArthur et al. 2003), many of the blobs are best fit by classic de Vaucouleurs ( $n = 4$ ) profiles. The same is true of POX 52 (Thornton et al. 2008).

It is not completely clear that single-component models are a good fit for all of the blobs. Particularly in the case of GH04 and GH12 there appears to be a compact ( $\sim 0''.15 - 0''.3$  or hundreds of pc at the distance of these sources) residual. There are a variety of possible explanations for this component. The most natural is PSF mismatch, since there is real structure in the PSF on this scale. However, the compact residuals persist in these two systems when we perform the fits on the smoothed images, suggesting that PSF mismatch is not the culprit. If this is indeed a physical component, we note that it is significantly more extended than the nuclear star clusters that appear to be a common component of the nuclei of galaxies of both late (e.g., Böker et al. 2002) and early type (e.g., Carollo et al. 2002;

<sup>5</sup>There are two galaxies for which this distinction was not obvious. GH11 is morphologically disturbed but is best fit as a compact disk (see Appendix), while GH15 is simply very faint. There is really no preference between the  $n = 1$  and  $n = 2$  models for GH15, but the former has a marginally smaller  $\chi^2$ .

Table 2. Host Galaxy Structure

Non-parametric					Parametric											
Name (1)	AGN		Galaxy		AGN		$n$ (8)	Bulge		Disk		Bar		Galaxy		
	$m_B$ (2)	$B-I$ (3)	$m_I$ (4)	$B-I$ (5)	$m_B$ (6)	$B-I$ (7)		$m_I$ (9)	$r_e$ (10)	$m_I$ (11)	$r_e$ (12)	$m_I$ (13)	$r_e$ (14)	$B/T$ (15)	$B-I$ (16)	$M_I$ (17)
GH01	20.2	1.0	17.0	2.1	20.3±0.2	1.1±0.3	1	17.5±0.3	0.8±0.1	17.8±0.3	3.0± 3.3	...	...	0.56	2.3	-20.8
GH02	20.9	1.5	15.1	1.8	20.7±0.4	0.3±1.6	2	17.2±0.3	0.9±0.2	15.1±0.1	7.4± 0.7	...	...	0.12	2.0	-20.6
GH04	19.5	1.2	16.6	1.8	20.2±0.3	0.4±1.6	4	16.5±0.1	0.66±0.03	...	...	...	...	1.00	1.9	-19.9
GH05	19.5	0.9	17.1	2.2	19.5±0.1	-0.4±3.2	...	<20.5	<0.1	17.2± 0.2	1.6± 0.4	19.2±0.8	0.5±0.4	<0.05	2.4	-20.6
GH06	21.3	1.2	18.1	2.2	21.2±0.1	0.5±1.1	...	<19.3	<0.2	18.0±0.1	1.3±0.1	...	...	<0.24	2.3	-20.3
GH07	20.7	1.2	17.9	2.2	20.6±0.1	0.0±1.7	3	17.6±0.4	1.8±0.5	...	...	...	...	1.00	2.1	-20.5
GH08	19.2	0.9	16.1	1.9	19.2±0.1	0.2±1.2	...	<19.0	<0.2	16.3± 0.1	3.3± 0.3	17.9±0.1	2.0±0.1	<0.07	1.9	-21.7
GH09	21.3	1.9	17.1	3.0	21.4±0.1	0.9±1.2	4	16.9±0.2	1.4±0.3	...	...	...	...	1.00	3.0	-23.0
GH10	19.2	1.1	17.0	1.9	19.5±0.1	-0.5±2.8	4	16.8±0.1	0.6±0.1	...	...	...	...	1.00	2.0	-21.0
GH11	21.4	2.0	17.1	1.7	22.3±3.0	2.1±3.0	...	<18.9	<0.2	17.2±0.1	0.5±0.1	...	...	<0.17	1.8	-20.6
GH12	19.6	1.1	17.8	2.1	19.6±0.1	0.1±1.4	4	17.6±0.2	1.3±0.3	...	...	...	...	1.00	2.4	-20.8
GH13	19.9	1.0	16.5	1.8	19.8±0.1	0.2±1.3	...	<20.3	<0.1	16.9± 0.1	3.0± 0.3	19.4±0.1	1.2±0.1	<0.04	2.0	-22.1
GH14	20.8	1.4	14.4	1.8	21.8±2.3	1.0±2.9	2	17.5±0.2	0.37±0.05	14.1±0.1	7.3± 0.7	...	...	0.04	1.9	-21.4
GH15	20.9	1.4	19.5	2.5	20.8±0.1	0.4±1.5	...	<22.4	<0.02	19.5±0.1	0.5±0.1	...	...	<0.07	2.6	-19.3
GH16	20.1	1.3	16.9	2.0	20.3±0.2	0.4±1.4	2	16.9±0.3	0.83±0.02	...	...	...	...	1.00	2.1	-20.5
GH17	20.3	1.2	18.0	2.2	20.2±0.1	0.3±1.5	2	18.0±0.4	1.1±0.1	...	...	...	...	1.00	2.2	-20.3
GH18	21.4	1.0	17.8	2.2	21.3±0.1	0.3±1.1	...	<21.0	<0.1	17.8±0.1	1.9±0.2	...	...	<0.05	2.3	-22.0
GH19	21.4	1.9	15.5	2.0	22.0±0.5	1.0±2.2	2	17.6±0.6	0.8±0.5	15.5±0.1	5.0± 0.5	...	...	0.13	2.1	-20.6

Note. — Col. (1): Object name from Greene & Ho 2004. Col. (2): Non-parametric  $B$ -band AGN magnitude using a scaling to the inner four pixels. Col. (3): Non-parametric  $B-I$  AGN color (mag). Col. (4): Non-parametric total galaxy magnitude in  $I$ . Col. (5): Non-parametric  $B-I$  galaxy color (mag). Col. (6): Parametric  $B$ -band AGN magnitude. Col. (7): Parametric  $B-I$  AGN color (mag). Col. (8): Sérsic index for the bulge component when detected in the best GALFIT model. Col. (9): Bulge  $I$  magnitude or upper limit. Col. (10): Bulge effective radius (") in  $I$ . Col. (11): Disk  $I$  magnitude, when present. Col. (12): Disk effective radius (") in  $I$ . Col. (13): Bar  $I$  magnitude, when present. Col. (14): Bar effective radius (") in  $I$ . Col. (15): Bulge-to-total luminosity ratio. Col. (16): Parametric  $B-I$  galaxy color (mag). Col. (17): Total absolute  $I$ -band magnitude.

Côté et al. 2006). Nuclear rings of star formation can be this size (e.g., Buta & Combes 1996), and the colors of GH04 and GH12 are bluer than typical elliptical galaxies. Interestingly, Thornton et al. (2008) also see evidence for a similar component in the  $B$ -band image of POX 52. Given the potential complications of PSF mismatch, we are wary of overinterpreting the physical significance of the residuals.

While the blob images do not present any compelling visual evidence for an additional exponential disk, we wish to place limits on the presence of such a component. There is an infinite family of possible low surface brightness disks, but normal disks do not span this entire space. Rather, there is an empirical correlation between disk scale length and bulge size. This correlation has been seen in a various studies (e.g., Courteau et al. 1996; de Jong et al. 1996b; MacArthur et al. 2003), at a variety of wavelengths, and over a broad range in Hubble type. By constraining the putative disk component to obey these scalings we can place limits on the existence of typical disk components in the blob galaxies.

Since our galaxies are relatively faint, we use the relation from MacArthur et al. that was calibrated for late-type spiral galaxies;  $\langle r_e/h \rangle = 0.22 \pm 0.09$ , where  $r_e$  is the effective radius of the bulge and  $h$  is the scale length of the disk (and the effective radius of the disk,  $r_d = 1.678h$ ). In addition to the scatter in the relation, there is significant uncertainty in the real blob parameters. Folding in all of these uncertainties yields a maximum and minimum disk size. At the same time, we need to assign a central surface brightness to each disk; we use the relation between bulge and disk surface brightness shown in Fig. 19 of de Jong (1996b) with a magnitude of scatter in each direction. In converting between  $B$  and  $I$ , we use a color  $B-I = 1.67$  mag for Scd galaxies (Fukugita et al. 1995). Each size and central luminosity corresponds to a well-defined radial profile, assuming an exponential disk and an inclination of  $45^\circ$ . To test the detectability of this disk, we simply calculate the radius at which the surface brightness of the disk and blob are equivalent. As long as that radius is within the limiting radius at which we de-

tect the blob (as determined from the radial profiles in Fig. 1), we would detect the disk if it were present. By this criterion, all the simulated disks are detectable and therefore we can state rather strongly that the blob galaxies do not have a “normal” disk component. Note that it is much harder to limit the presence of a face-on disk. In that case we still might expect to see spiral structure in the fit residuals, which we do not.

#### 4.2. Disk Galaxies

The basic approach is similar for the disk galaxies. In this case there is less degeneracy between the nucleus and the disk, which is not centrally concentrated. The best-fit disk is determined from GALFIT with the Sérsic index fixed to 1. As a first pass, we fit only a disk component. If there is a visible bar, as in the case of GH05, GH08, and GH13, we then take the best-fit disk and add a bar with a Sérsic index fixed to 0.5, which is equivalent to a Gaussian (e.g., de Jong 1996a). In some other cases (GH01, GH02, GH14, GH19), there is a clearly resolved bulge component, whose addition yields a dramatic improvement in  $\chi^2$ . In other cases (GH06, GH18), although there are hints of a bulge component in the residuals, the component is only marginally resolved and we do not achieve stable fits with GALFIT. For these cases, and those whose nuclei are dominated by the bar, we place limits on the bulge component. We note that in many cases the disk galaxies in particular show substantial structure in the residual images, typically corresponding to spiral arms, which we do not fit (in some cases, such as GH08, it is also clear that our bar model is not perfect).

For those systems without a clearly resolved bulge, our general approach is similar to the case of the blobs. Again, our strategy is to limit the presence of a typical bulge, i.e. one that obeys the scaling relations seen in inactive galaxies. We use the same correlation between disk scale length and bulge effective radius from MacArthur et al. (2003), and we further insist that the bulge lies on the fundamental plane. There are three bulge models that span the range of sizes allowed by the measured disk-bulge size relation, and from these sizes we assign a lumi-

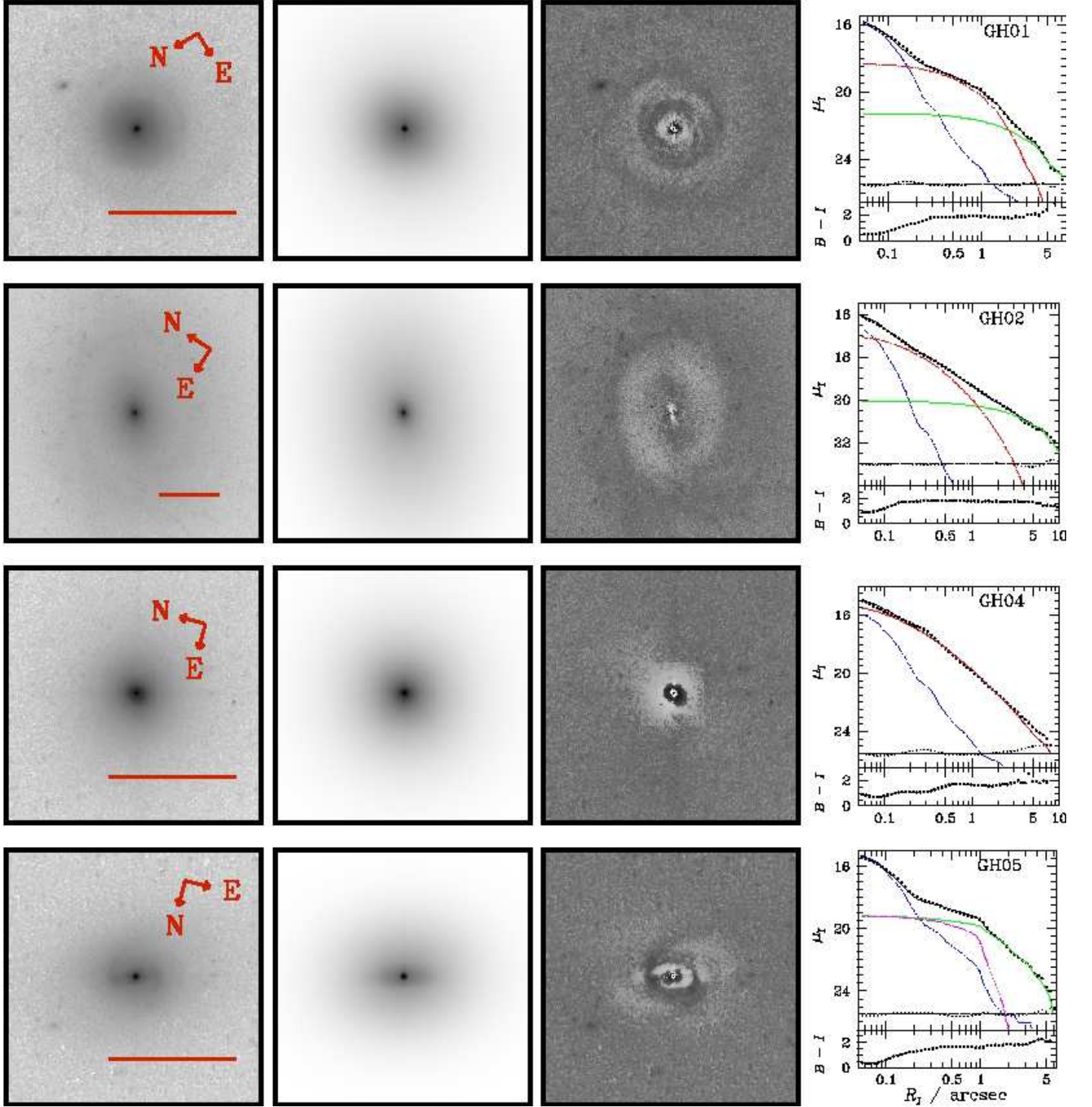


FIG. 1.— *HST* images presented in this paper. From left to right we display the *I*-band image, the preferred GALFIT model, the residuals, and an azimuthally averaged profile created with the IRAF program *ellipse*. Scale bar represents 5". In the two-dimensional residuals there is often a nearly vertical artifact caused by diffraction spikes in the star used to model the AGN. Plotted in the one-dimensional residuals are the data (filled circles), the total model (solid line), the AGN (blue long-dash-dotted line), and, if present, a bulge (red dotted line), a disk (green dash-dot line), and bar (magenta dash-dot line). The fit residuals are shown as small dots. In the bottom panel we show the  $B-I$  color profile of the galaxy, including the AGN.

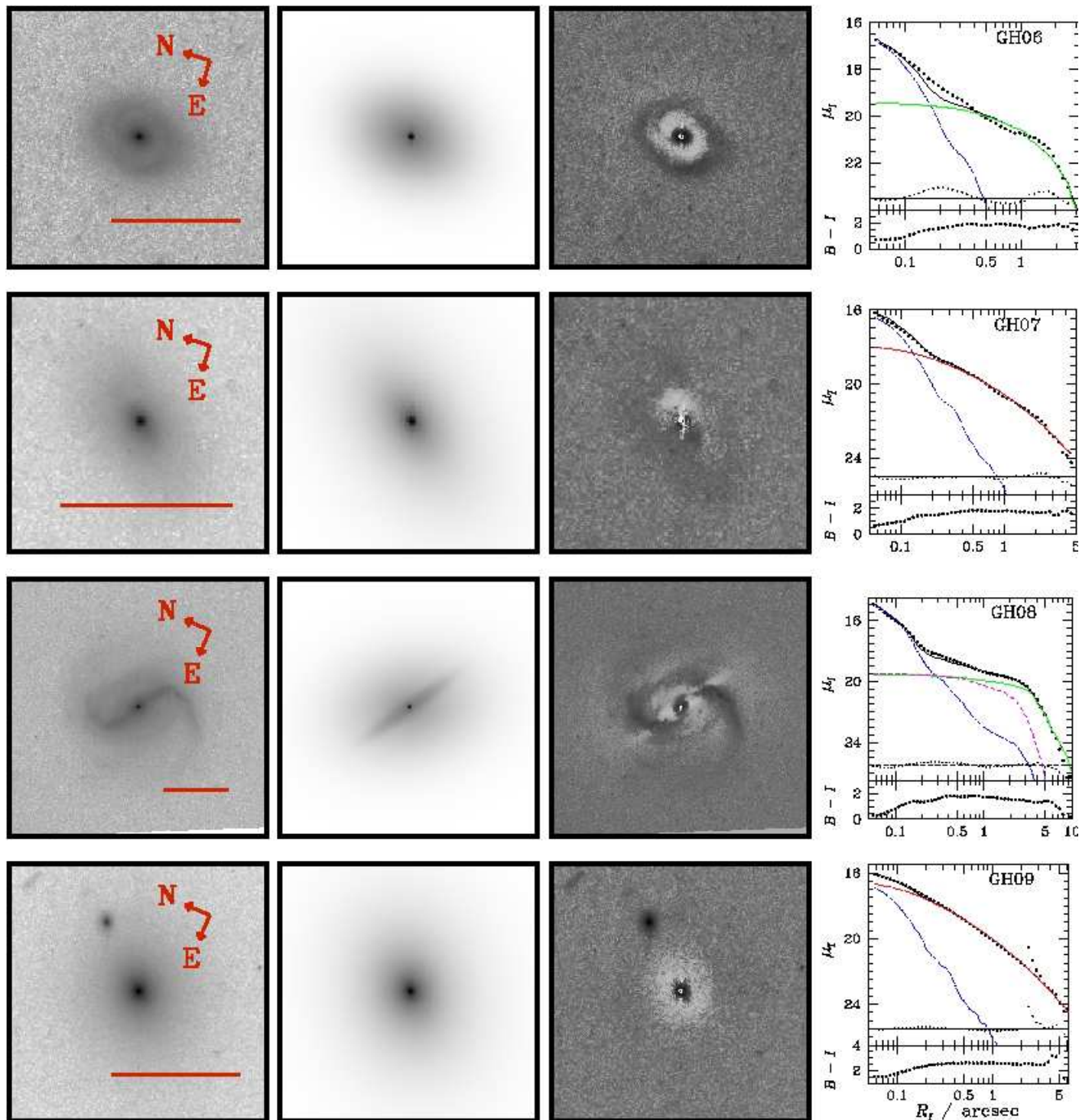


Fig. 1. — continued.

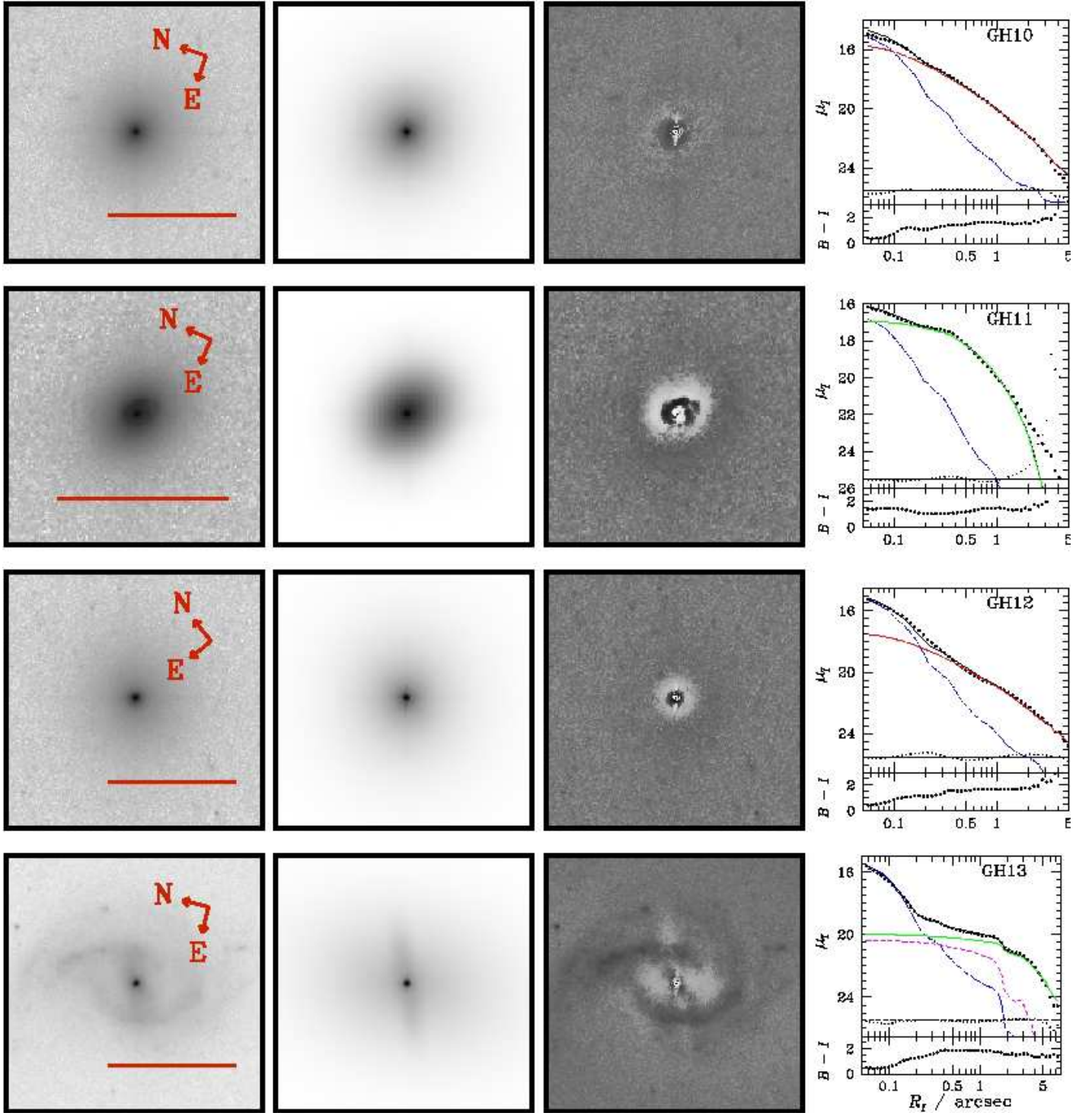


Fig. 1. — continued.

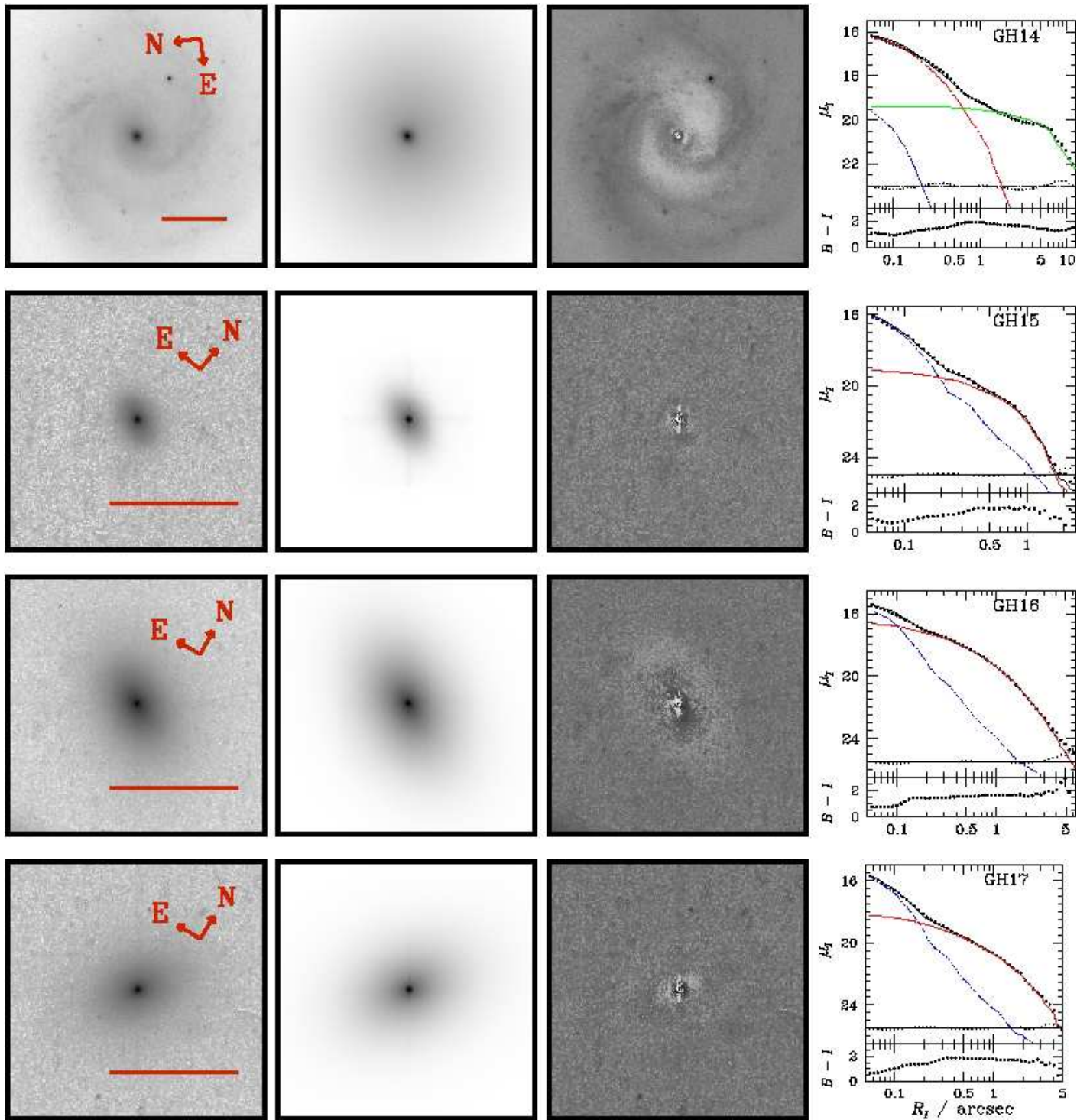


Fig. 1. — continued.

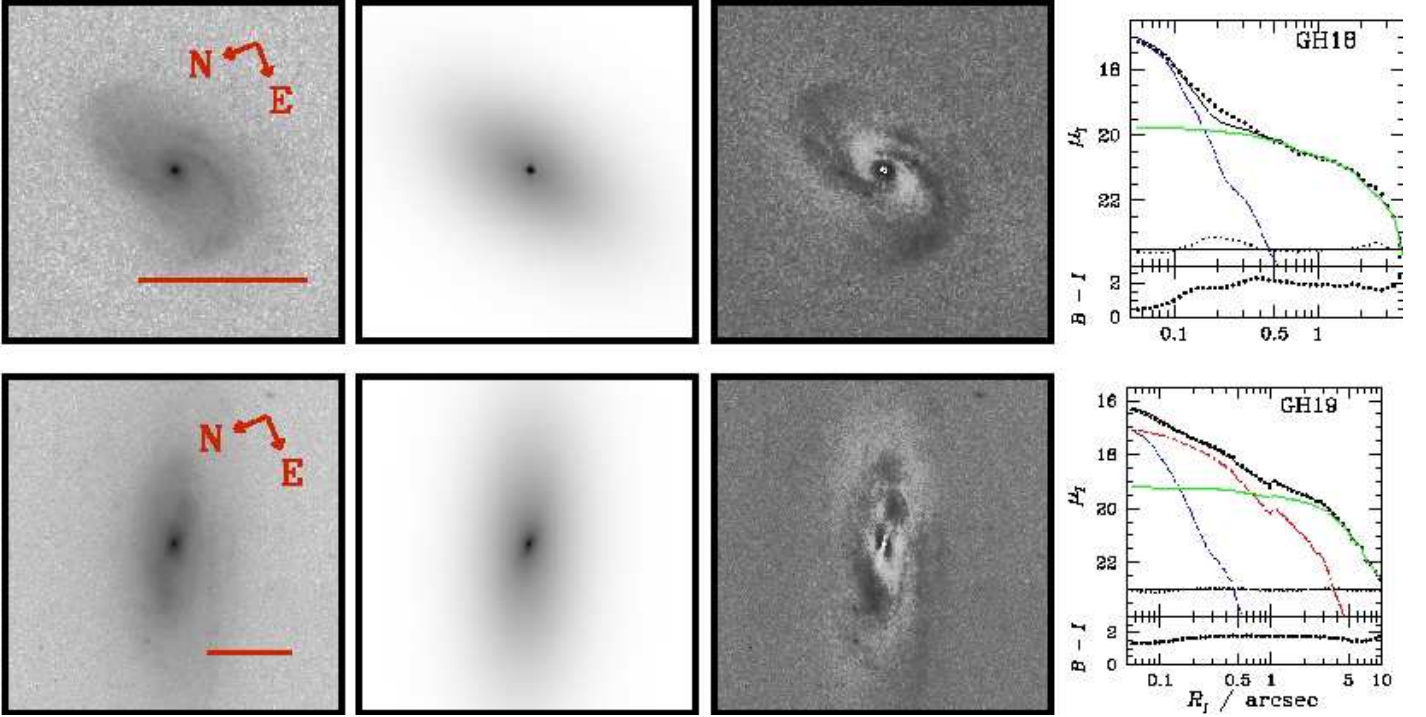


Fig. 1. — continued.

nosity using the fundamental plane projections of Bernardi et al. (2003), assuming a color transformation of  $i' - I = 0.63$  mag. We repeat the fitting process including a bulge with the sizes and luminosities fixed to the values thus determined, and the spatial position, axial ratio, and position angle fixed to that of the disk. For increased sensitivity to changes in the model on the scale of the bulge, we calculate two  $\chi^2$  statistics from the radially averaged profiles. The first uses all of the data, while the second is limited to radii ranging from the effective radius of the putative bulge to the measured effective radius of the disk. This is designed to maximize our sensitivity to the regime in which light from the bulge would dominate, if present. In most cases the  $\chi_r^2$  is close to unity for the total radial profile, and in all cases the extra component makes a large impact on the fits (sometimes improving it). We adopt as the bulge upper limit the largest (most luminous) bulge that cannot be ruled out from the fitting. The most important outcome of this exercise is that we are unable to rule out the presence of a reasonably sized bulge-like component in any of the galaxies.

We now have structural measurements (size, luminosity, and surface brightness) or upper limits for the bulge-like components of all the galaxies in our sample, and  $\sigma_*$  measurements for most of them. In principle we can also derive color gradient information, which may significantly impact our inferences about galaxy structure. For instance, a nuclear starburst would make the galaxy appear more centrally concentrated than it truly is. Unfortunately, the inner 200 pc of our images are dominated by the AGN. The combination of uncertainties in PSF shape (particularly in the blue) and centroiding errors make it prohibitively difficult to extract believable color information in the inner regions. Before turning to an investigation of the fundamental plane properties of these systems, we now briefly investigate the most pernicious sources of systematic uncertainty and their magnitudes.

#### 4.3. Uncertainties

In this section we attempt to isolate the model assumptions and parameters that potentially contribute most significantly to the error budget for each fit. The first is small errors in the sky estimation that can lead to significant errors in magnitude and size measurements. To quantify the uncertainties due to sky level, we simply rerun each GALFIT model with the sky level fixed at  $\pm 1 \sigma$  of the best-fit value, where  $\sigma$  is determined from four well-separated regions of 200 square pixels each, and is typically at the 1% level but never exceeds 2%. The resulting dispersion in parameter values is added in quadrature to the total error budget of each parameter. Typically the sky-related uncertainties are at the 10% level in radius, although they are closer to 30% for the bulges in disk galaxies, and  $< 0.1$  mag in luminosity.

More difficult to quantify are uncertainties in the PSF model. As discussed above, while the *HST* PSF is very stable, nevertheless it displays both temporal and spatial variations (e.g., Rhodes et al. 2007), and errors in the assumed PSF will translate into errors in the inferred galaxy structural parameters. Our approach is to use multiple PSF models, derived both from bright stars in our fields and from TinyTim, with the hope that the differences in the fits represent the uncertainties incurred by imperfections in our model. However, if there is something systematically incorrect in all of our PSF models, then we can underestimate the true errors. One way to more robustly quantify the impact of PSF variations is to perform simulations in which the PSF model is changed in controlled ways. M. Kim et al. (in preparation) have run a suite of simulations investigating the impact of spatial, temporal, and color variation on the resulting fits. For simulations in which the host luminosity is  $\sim 10$  times larger than the nuclear luminosity, which is the case for the red images, PSF mismatch does not impact the host galaxy fits substantially. Indeed, we find the variation in structural parameters from different PSF models to be small ( $< 10\%$ ,

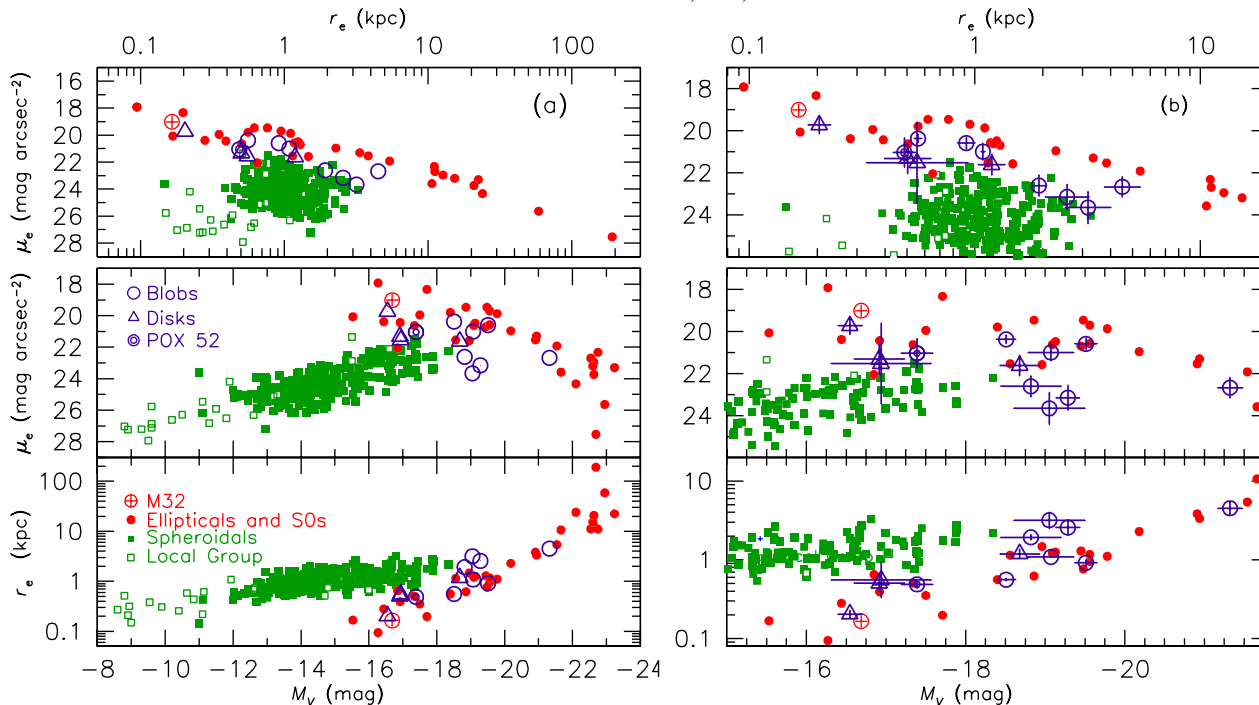


FIG. 2.— (a): The fundamental plane of hot stellar systems from the recent study of Kormendy et al. (2008), predominantly for Virgo cluster galaxies. We show elliptical and S0 galaxies (filled red circles), Virgo spheroidal galaxies (filled green squares; from Kormendy et al. 2008, supplemented by Ferrarese et al. 2006 and Gavazzi et al. 2005) and Local Group dwarf spheroidal galaxies (open green squares; Matteo 1998; McConnell & Irwin 2006). Our systems are shown as open blue symbols, with the blobs as circles and the disks with detected bulges as triangles. POX 52 comes from the recent *HST* measurements of Thornton et al. (2008). Bulge upper limits are not included. (b): The same figure enlarged to highlight the region where our objects are found.

with the exception of the bar parameters). At the same time, the spread in *I*-band AGN magnitudes from different PSF stars can be as large as two magnitudes.

Although it is rarely discussed, Kim et al. point out that PSF undersampling causes errors in centering that in turn lead to systematic fitting errors. While it is somewhat counterintuitive, broadening both the PSF model and the image slightly can mitigate the impact of undersampling. Therefore, we have repeated the fits on images smoothed with a Gaussian kernel with  $\sigma = 2$  pixels in both *x* and *y*. As expected, we find minimal changes to the host galaxy properties, and this error contributes least to the error budget of the structural parameters, but we do see typical variations in the PSF magnitudes of  $\sim 0.2$  mag. We add this uncertainty in quadrature to the errors of both the PSF and host galaxy models.

Finally, the hardest systematic uncertainties to quantify are those due to our model assumptions, since in detail galaxies need not be well-described by a single Sérsic model. Even in the absence of a nuclear point source, profile decomposition is a tricky game rife with degeneracy (see, e.g., discussion in MacArthur et al. 2003). We have tried to be conservative in our error estimation by including the range of measured properties from a wide range of Sérsic indices. However, it is clear that in at least a few cases our models are not completely adequate. In addition to the clear nuclear residuals in GH04 and GH12, GH11 also has well-resolved ring-like residuals. It is difficult to quantify the systematic errors associated with incorrect models. One thing we can say is that the total luminosities are robust, based on comparisons with the non-parametric measurements. The galaxy magnitudes show good agreement between the two methods, with a median magnitude difference of  $0.1 \pm 0.2$  mag in *I*, and a median color difference of  $-0.01 \pm 0.3$  mag. Even the AGN magnitudes agree well. In *B*, the median magnitude

difference is  $0.04 \pm 0.4$  mag. The agreement is not as good in the *I* band, where the galaxy often constitutes a significant fraction of the total light within the inner two pixels; the median non-parametric AGN magnitude is  $1 \pm 0.4$  mag brighter than the parametric fit. This is why we use the *B*-band fits to measure the AGN magnitudes.

## 5. HOST GALAXY SCALING RELATIONS

### 5.1. The Fundamental Plane

Our goal is to use the fundamental plane to determine the structural family (and thus formation history) of the AGN host galaxies. Although there is a rich morphological diversity across late-type galaxies in the luminosity range of our sample, conceptually we wish to distinguish between two basic formation scenarios. On the one hand, the structural similarity of elliptical galaxies and classical bulges presumably reflect a violent merger history (e.g., Burstein et al. 1997; Robertson et al. 2006). On the other hand, more quiescent evolution probably results in disk-like galaxies, either containing pseudobulges or (when the gas and outer regions have been removed) with the structure of spheroidal galaxies (e.g., Kormendy & Kenicutt 2004; Kormendy et al. 2008). Figure 2a beautifully illustrates the discriminatory power provided by projections of the fundamental plane. The projections are defined by a very clean sample of elliptical and spheroidal galaxies in the Virgo cluster, representing the most careful and modern photometric measurements available from the recent study of Kormendy et al. (2008). While the positions of pseudobulges are less certain, Carollo (1999) shows that pseudobulges also may have a lower surface brightness at a given size than classical bulges.

Using our structural measurements, and assuming  $V - I = 1.34$  mag (from Fukugita et al. 1995, to match the Sa colors of the galaxies, see below), we place our targets in the funda-

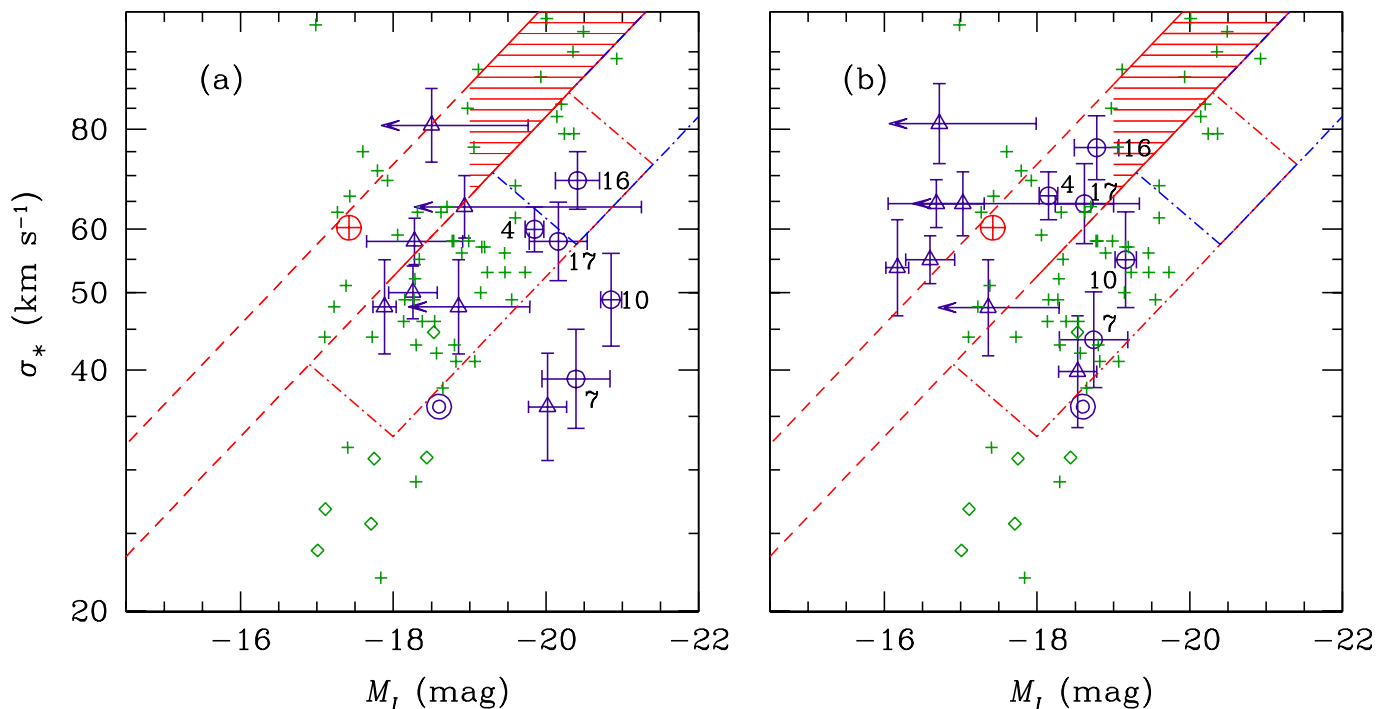


FIG. 3.— (a): Faber-Jackson projection of the fundamental plane. As above, our galaxies are shown as open blue symbols, with circles for blobs and triangles for the disk galaxies with detected bulge components. The inactive relation for elliptical galaxies and classical bulges from Bernardi et al. (2003; assuming  $i-I = 0.63$  mag) is shown as the red shaded region, while the extrapolated region is shown as dashed lines. Two samples of spheroidal galaxies are shown for comparison, Geha et al. (2002; *green diamonds*, assuming  $V-I = 1.34$  mag) and Matković & Guzmán (2005; *green crosses*, assuming  $B-I = 1.8$  mag). From the data compilation in Kormendy & Kennicutt (2004), it appears that the relation may not be linear at the lowest luminosities, but rather depart toward lower  $\sigma_*$  at a given luminosity, as shown schematically by the red box in dash-dot. Finally, from the same compilation we indicate the region occupied by pseudobulges with a blue rectangle. (b): Same as (a), except that we have corrected the velocity dispersions for the potential influence of either a nuclear star cluster or a face-on disk component. Furthermore, we have aged the stellar populations using an evolutionary correction to the luminosities and average surface brightnesses of the galaxies, which we argue represents the maximum amount of fading and incorporates a reasonable reddening estimate (see text for details).

mental plane (Fig. 2, *open blue symbols*). We plot only the bulge components of the fit, comprising the entire galaxy in the case of the blobs, but only the compact central component in the case of the disk galaxies. We exclude the bulge upper limits from Figure 2 since the upper limits on the bulges are derived assuming that they obey the Kormendy (1977) relation between surface brightness and effective radius. Most likely, given the luminosities and morphological types of these systems, as well as the upper limits on their bulge-like components, these seven systems contain pseudo- rather than classical bulges.

We see first of all that while our galaxies are fainter than  $L^*$  ( $I^* = -21.5$  mag at  $z = 0.1$  from Blanton et al. 2003b and assuming  $i' - I = 0.63$  mag), they are typically a magnitude brighter than the tip of the spheroidal sequence. In terms of structures, we see that while some of the blobs obey the fundamental plane of classical bulges (GH04, GH09, GH10, and GH16), others are significantly offset toward the locus of spheroidal galaxies (GH07, GH12, and GH17). The detected bulges, with the exception of GH14, have structures more similar to spheroidal galaxies, as expected for pseudobulges (e.g., Carollo 1999). POX 52, while faint enough to overlap with the spheroidal sequence, is more centrally concentrated than typical for a spheroidal galaxy, as supported by the high Sérsic index,  $n = 4.3$ . At the same time, POX 52 also shows evidence for a spatially resolved central component in the  $B$ -band (Thornton et al. 2008). Such a component would preferentially boost the central surface brightness and decrease the effective radius, but when the young component fades it may move onto the spheroidal sequence. We see tentative evidence for a similar component in GH04. Thus the photometric projections alone

are rather ambiguous. Let us turn now to the stellar velocity dispersions, which provide additional constraints on the nature of these galaxies.

In Figure 3a we present the Faber-Jackson (1976) relation for inactive elliptical galaxies from Bernardi et al. (2003), along with the locations of two spheroidal samples (Geha et al. 2002; Matković & Guzmán 2005). Taken at face value virtually none of our galaxies obeys the Faber-Jackson relation of elliptical galaxies, but there are a couple of significant complications to the interpretation. First of all, it is unclear whether low-luminosity ellipticals have a linear Faber-Jackson relation, as illustrated schematically in Figure 3 (see Kormendy & Kennicutt 2004). There may be a downturn in  $\sigma_*$  at low luminosities, making the spheroidal, pseudobulge, and elliptical sequences overlap in this regime. At the same time, we cannot be sure that the dispersion measurements are dominated by stars in the bulge component. If there is a bright nuclear star cluster or significant luminosity from a face-on disk, light from these stars will artificially lower our luminosity-weighted stellar velocity dispersion measurement. Indeed, the significant offset in the Faber-Jackson relation for the sample as a whole, independent of position in the photometric projections, is somewhat worrisome. An additional factor that will move objects in the Faber-Jackson plane, of course, is the mix of stellar populations. In the following section we estimate the impact of stellar populations and aperture size on our measurements.

## 5.2. Impact of Stellar Evolution, Dust Reddening, and Stellar Kinematics

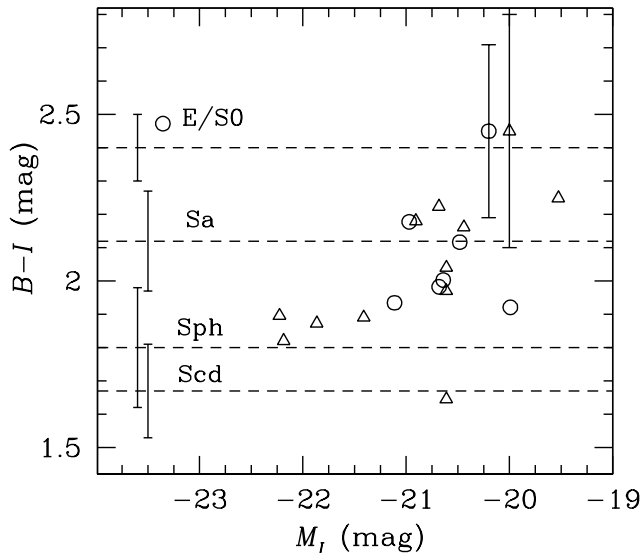


FIG. 4.— Host galaxy location in a color-magnitude diagram. The colors are derived parametrically but agree with the non-parametric colors to within  $0.01 \pm 0.3$  mag. We use the entire galaxy (not just the bulge), but distinguish between blob (circles) and disk (triangles) galaxies. The relatively luminous and red galaxy is GH09. Representative error bars are shown for the blobs and disks respectively in the upper right-hand corner. For reference, the typical colors of E/S0, Sa and Scd galaxies are shown (dotted; Fukugita et al. 1995), and the spread in those colors are shown as error bars on the left-hand side of the plot. We also show the  $B-I$  color of spheroidal galaxies as estimated from Fig. 8 of Gavazzi et al. (2005) for systems with typical  $M_B \approx -14$  mag.

We first estimate the impact of young stellar populations on the observed luminosities. Because of relatively recent or on-going star formation, the luminosities of our galaxies cannot be compared directly with elliptical galaxies, which formed the majority of their stars at high redshift (e.g., Thomas et al. 2005). A truly fair comparison would require knowledge of their star formation histories and metallicity distributions, but full spectral synthesis modeling (e.g., Tinsley 1978) is difficult with only a single  $(B-I)$  color<sup>6</sup>. In particular, without near-infrared measurements, we do not have a strong handle on the magnitude of extinction, which is clearly playing a significant role. Figure 4 shows the observed location of our targets in the color-magnitude relation, along with the fiducial colors of galaxies of a variety of Hubble types (Fukugita et al. 1995). We can see that, with the exception of GH09, the galaxies are blue compared to elliptical galaxies. However, they are actually redder than we might have expected. For instance, GH05, GH08, and GH13 are late-type spiral galaxies with bulge-to-total luminosity ratios  $B/T < 0.07$  and yet their  $B-I$  colors are redder than that of a typical, bulge-dominated Sa galaxy, presumably because of reddening.

In the absence of more detailed information, we use a very simplistic prescription to account in an average way for the combined impacts of reddening and stellar evolution on the observed color. For all galaxies in the sample we simply assume a single intrinsic color of  $B-I = 1.67$  mag. This color is typical of Scd galaxies (Fukugita et al. 1995) and is close to the typical color of spheroidal galaxies in the Gavazzi et al. sample,  $B-I \approx 1.8$  mag. From this one assumption, we can then derive both the reddening and (with the further assumption of a sin-

gle stellar population) the total stellar mass. While we are not adequately recovering the star formation history of individual galaxies in our sample, this simple thought experiment provides an estimate of the impact of young stellar populations on the ensemble. As we will show below, more sophisticated modeling yields similar final results.

Given our assumed intrinsic color, we first derive the reddening for each galaxy assuming  $A_B/A_V = 1.32$  and  $A_I/A_V = 0.59$ , as derived by Schlegel et al. (1998) using the reddening curves of O'Donnell (1994; optical) and Cardelli et al. (1989; ultraviolet and near-infrared). We find typical  $A_I$  values of  $\langle A_I \rangle = 0.29 \pm 0.15$  mag, and have an estimate for the intrinsic luminosity of the system. Now, for the purpose of comparison, we ask what mass-to-light ratio ( $\Upsilon_I$ ) and stellar age are associated with a simple stellar population (SSP) with a color of  $B-I = 1.67$  mag. The synthesis model, from Bruzual & Charlot (2003), assumes a Chabrier (2003) initial mass function (IMF), solar metallicity, and uses the Padova 1994 stellar evolutionary tracks (Alongi et al. 1993; Bressan et al. 1993; Fagotto et al. 1994a,b; Girardi et al. 1996). The SSP has a color of  $B-I = 1.67$  mag at an age of  $2 \times 10^9$  yrs and  $\Upsilon_I = 0.6$ . The decrease in luminosity associated with an increase to  $\Upsilon_I = 3.7$  (the final  $\Upsilon_I$  for this model at an age of  $2 \times 10^{10}$  yrs) corresponds to  $\Delta m_I = 1.9$  mag. Combining the effects of reddening and stellar aging yields an absolute  $I$ -band magnitude and an average surface brightness for each target, corresponding to a typical magnitude change of  $\langle \Delta m_I \rangle = 1.6 \pm 0.2$  mag. Using the inferred reddening and measured luminosity, and assuming an SSP, we not only estimate the magnitude of aging, we also infer a total stellar mass for each system.

Crucially, our approach is designed to yield an upper limit to the impact of stellar aging. This is because undoubtedly the galaxies contain a significant evolved population that boosts the current mass-to-light ratio. For instance, *kcorrect* (Blanton et al. 2003a; Blanton & Roweis 2007) models a wide range of star formation histories, metallicities, and reddening values, and returns  $\Upsilon_I$  values of 1.1–1.4 for the galaxies (using either the *HST* color, or the SDSS magnitudes corrected for the nuclear point source using the *HST*  $B$ -band measurement), implying fading of  $\Delta m_I = 1 - 1.3$  mag. Furthermore, particularly for the blobs, the assumed intrinsic color may be too blue; a color of 1.8–2 mag may be more appropriate (e.g., Geha et al. 2002; Gavazzi et al. 2005)<sup>7</sup>.

The stellar kinematics also impact the observed Faber-Jackson relation. Although we wish to know the integrated velocity dispersion of stars in a dynamically hot stellar component within an effective radius ( $\sigma_*$ ), what we measure ( $\sigma_{*m}$ ) is the luminosity-weighted mean dispersion of all of the stars in our aperture. If the stars are rotation-dominated (e.g., in a nuclear disk) then we will measure broadening due to unresolved rotation. If the light is dominated by stars in a face-on disk, then  $\sigma_{*m}$  will underestimate the true dispersion. Furthermore, our spectroscopy is not performed out to the effective radius, but rather within a  $0''.7$  slit corresponding roughly to  $r_e/2$  for most of the sample (ranging from 20%–90% of  $r_e$ ; Barth et al. 2005). Apart from broadening due to unresolved rotation, we might either systematically over- or underestimate the true dispersion depending on the velocity dispersion profile.

<sup>6</sup>Although in principle additional information may be extracted from the ESI spectra, the difficulties in modeling the combination of an AGN and mixed stellar populations with the additional complications of imperfect flux calibration and slit losses make such an analysis beyond the scope of the current work.

<sup>7</sup>Additional complication is certainly added by the spatial distribution of the star formation. One might expect nuclear star formation associated with AGN activity, and perhaps we are seeing that in the cases of GH04 and GH12. On the other hand, in the spiral galaxies the star formation may occur preferentially in the outskirts.

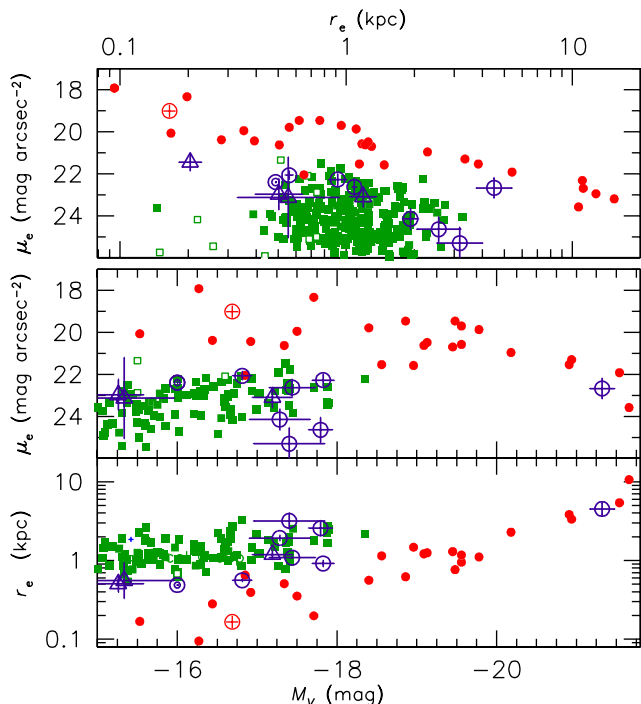


FIG. 5.— A reproduction of the fundamental plane projections shown in Figure 2 with our simplistic estimates for the stellar population fading applied.

At large radius, radial  $\sigma_*$  profiles are quite flat for elliptical galaxies (e.g., Jørgenson et al. 1995) and spiral bulges (e.g., Pizzella et al. 2005). At  $r \ll r_e$ , however, the profiles are more diverse. For instance, in the SAURON sample, the luminosity-weighted mean stellar velocity dispersion at  $0.1r_e$  is  $\sim 20\%$  higher than at the effective radius (Cappellari et al. 2006). In spheroidal galaxies, conversely,  $\sigma_*$ -drops of  $> 30\%$  are commonly observed (e.g., Geha et al. 2002; van Zee et al. 2004; De Rijcke et al. 2004, 2006). On the other hand, at  $r \approx 0.5r_e$ , the impact of these excursions is actually minor. The Cappellari et al. profiles show that  $\sigma_*$  at  $0.3r_e$  is already within 10% of  $\sigma_*$  at  $r_e$ . Likewise, the Geha et al. profiles have already flattened at a few tenths of  $r_e$ .

Empirically, if the  $\sigma_{*m}$  values are depressed due to a drop toward the center, then sources that we observed at the lowest fraction of  $r_e$  should have the largest deviations from the Faber-Jackson relation. Even including the disks with only bulge upper limits, which in general lie closer to the Faber-Jackson relation, we find no evidence for a correlation between  $r/r_e$  and Faber-Jackson offset; a Kendall's  $\tau$  test indicates a 70% probability that no correlation is present. Alternatively, the galaxies with the most prominent blue centers (and therefore the strongest nuclear weighting of a possible cold component) may show the largest deviations from Faber-Jackson. However, we see no significant correlation between either the integrated parametric color or an inner color, with a 30% chance of no correlation. The inner color is measured from the raw data between the radius where the model is more than twice the luminosity of the AGN and the effective radius of the bulge (or disk in the case of upper limit systems).

Although we see no obvious trends between offsets in the Faber-Jackson plane and either our aperture or the galaxy color, we now make simple estimates of the relative contribution to  $\sigma_{*m}$  from a non-bulge component. We begin with a hypothetical nuclear stellar concentration in the blob systems by assign-

ing 50% of the AGN luminosity to a nuclear star cluster with a velocity dispersion that is 60% of the assumed  $\sigma_*$  at larger radius. We then compute the luminosity-weighted dispersion within our aperture using the measured light profile and assuming a constant  $\sigma_*$  outside of the unresolved nucleus. In general the contamination to  $\sigma_*$  is small, but  $\sigma_{*m}$  can be depressed by as much as 10% compared to the assumed true  $\sigma_*$ .

In particular for the disk systems, we worry that  $\sigma_{*m}$  may be dominated by unresolved rotation. Again, a disk component may increase or decrease  $\sigma_{*m}$  relative to  $\sigma_*$ , depending on whether the disk is closer to face-on or edge-on. Our images show that the disk-dominated galaxies are rather close to face-on, and so it is worth investigating the magnitude of  $\sigma_*$  depression that a kinematically cold disk component can cause, using our photometric decompositions. We calculate a one-dimensional luminosity-weighted stellar velocity dispersion, assuming a single value for the bulge component and  $10 \text{ km s}^{-1}$  for the disk (Bottema 1993). For the systems with detected bulges, the resulting contamination is small (5%–14%), whereas for those with bulge upper limits, the disk completely dominates the light at nearly all radii, and thus the corrections can be as large as 80%. At the same time, of course, rotation is likely to contribute significantly to  $\sigma_{*m}$  in these systems. Finally, we perform the same test with the blobs, using the disk limits derived in §4.1. In this case the corrections are very small ( $< 2\%$ ), since by definition we do not detect the disk significantly over the radii of our observations.

There is an additional factor that may impact the  $\sigma_*$  measurements, which is the presence of the AGN. As emphasized, e.g., by Greene & Ho (2006a), both narrow forbidden emission lines and broad Fe II pseudo-continuum can significantly bias  $\sigma_*$ , particularly in the Mg *Ib* spectral region. However, there are a variety of reasons to believe that these effects are minor in the case of this sample. The first is that for the  $\sim 50\%$  of the sample with calcium triplet measurements, Barth et al. (2005) find good agreement with the Mg *Ib* dispersions. Another is that the high resolution of the ESI data mitigates the contamination from emission lines. Finally, in general the sources are not strong Fe II emitters. Altogether, then, we suspect that the  $\sigma_*$  measurements are relatively free of bias from AGN contamination. In short, for the majority of cases we expect stellar contributions from a disk or compact component to depress  $\sigma_*$  at the 10% level, while for the three bulge upper limit systems, the dispersion is probably dominated by the disk component.

We now have crude estimates for the impact of both stellar population effects and stellar kinematics on the observed location of objects in the fundamental plane. We have attempted to derive the largest possible corrections, particularly in the case of stellar population aging, so that between the observations and our corrected values we bracket reality for all systems. Correspondingly, the maximum depression to  $\sigma_*$  that we derived for any of the blobs was 10%. In this spirit, and for schematic purposes only, Figure 3b shows the Faber-Jackson relation with the estimated stellar population evolution and the  $\sigma_*$  measurements boosted by 10% for the blobs. We also show the fundamental plane projections after fading in Figure 5.

What can we conclude then about the nature of the blobs? Based on the fundamental plane of Figure 2 alone, three of them (GH07, GH12, and GH17) look more like spheroidal galaxies that are abnormally bright due to ongoing star formation, while the other four are ambiguous. Their photometric structures look like elliptical galaxies, but their dispersions place them below

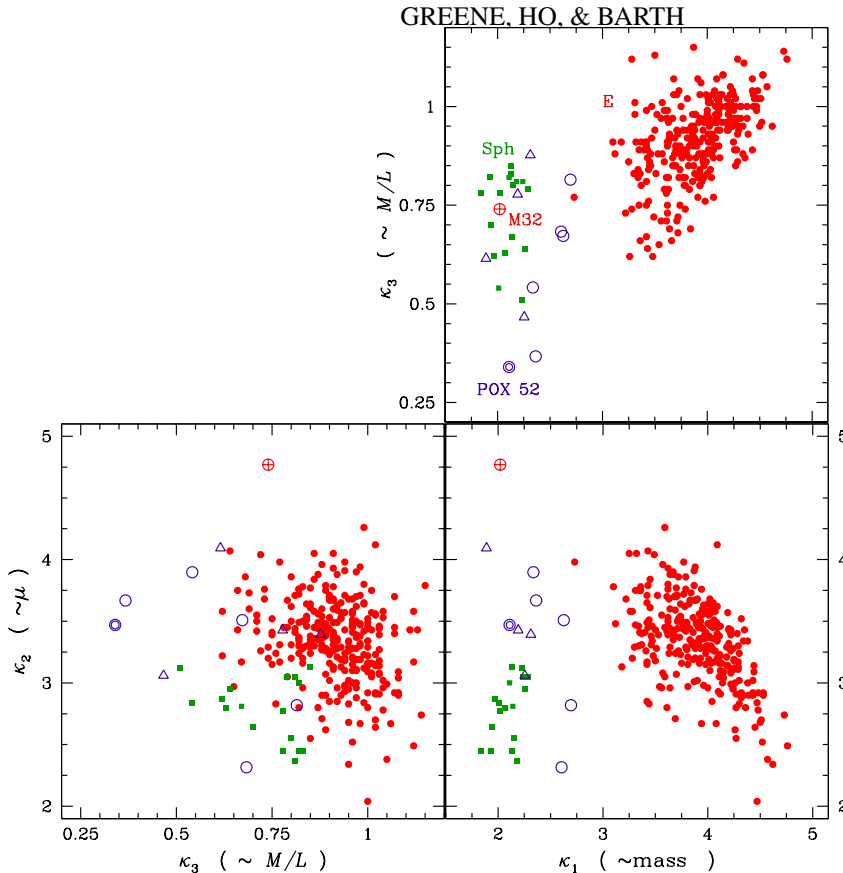


FIG. 6.—  $\kappa$ -space projections of the fundamental plane. Symbols as in Figure 2, with comparison data taken from the compilation of Bender et al. (1992) and Geha et al. (2002). We plot the observed data with no corrections here. In this space, our sample is clearly distinct from the locus of elliptical galaxies, mainly driven by the offsets in the Faber-Jackson plane.

the Faber-Jackson relation. It could be, as suggested by Kormendy & Kennicutt (2004), that Faber-Jackson is non-linear for low-luminosity elliptical galaxies, but much better statistics are needed to determine whether the effect is due to ongoing star formation or structural differences. We have shown that with reasonable assumptions about young stellar populations, the systems fade onto the spheroidal locus (Fig. 5). While GH09 is both too luminous and too red to be anything but an elliptical galaxy, we suspect that GH04, GH10, and GH16 will fade onto the spheroidal sequence. Thornton et al. (2008) draw similar conclusions about the nearby galaxy POX 52. While POX 52 has a high Sérsic index of 4.3, it is not exactly a scaled-down giant elliptical galaxy like M32; its low velocity dispersion of  $36 \text{ km s}^{-1}$  places it closer to the sequence of spheroidal galaxies (Figs. 3, 6).

To further emphasize this latter point, and as a convenient means of summarizing the fundamental plane results, we also present the “ $\kappa$ -space” formalism in Figure 6 (e.g., Bender et al. 1992). This is a coordinate transformation in which the axes are proportional to galaxy mass, surface brightness, and mass-to-light ratio, respectively (only galaxies with  $\sigma_*$  measurements can be included). It is clear that, due primarily to the offset in Faber-Jackson, our sample galaxies are significantly offset from the locus of elliptical galaxies in  $\kappa$ -space. In this formalism the blobs separate from the elliptical sequence in a similar fashion as inactive spheroidal galaxies.

### 5.3. Relations with BH Mass

We have identified a population of BHs in galaxies without classical bulges, strongly confirming that formation of the latter

is not a prerequisite for existence of the former. Nevertheless, given the different structural properties of the host galaxies, it is interesting to investigate whether the relationship between  $M_{\text{BH}}$  and  $L_{\text{bulge}}$  is preserved for this sample. The virial BH masses are directly compared with both the bulge luminosities (Fig. 7a) and bulge masses (Fig. 7b). These spheroidal and pseudobulge systems are striking outliers in the  $M_{\text{BH}} - L_{\text{bulge}}$  plane, in the sense that the galaxies are overluminous compared to the low-mass extrapolation of the  $M_{\text{BH}} - L_{\text{bulge}}$  relation. All of the blobs and detected bulges are offset independent of their location in the fundamental plane.

The observed offset is not an artifact of improper AGN-host galaxy decomposition. The AGN accounts for at most a few tenths of the total luminosity, and thus cannot be a major contributor to uncertainties in the galaxy magnitudes. It is, however, worth considering the possibility that the BH masses are systematically biased to low values. In the case of the blobs, if we wished to make the galaxies obey the  $M_{\text{BH}} - L_{\text{bulge}}$  relation the BH masses would need to be biased by 2 orders of magnitude on average. In principle it is possible that individual objects in the sample have considerably larger BH masses than suggested by their virial masses (as would occur, for instance, if the BLR were a face-on disk). We have shown, however, that the radiative properties of the sample are consistent with expectations for systems radiating at a high fraction of their Eddington limit [based on their optical (Greene & Ho 2004), radio (Greene et al. 2006), and X-ray (Greene & Ho 2007a) properties]. Thus, it is highly unlikely that these systems are actually, on average, radiating at  $< 1\%$  of their Eddington luminosities.

As with the fundamental plane, we speculate that the ob-

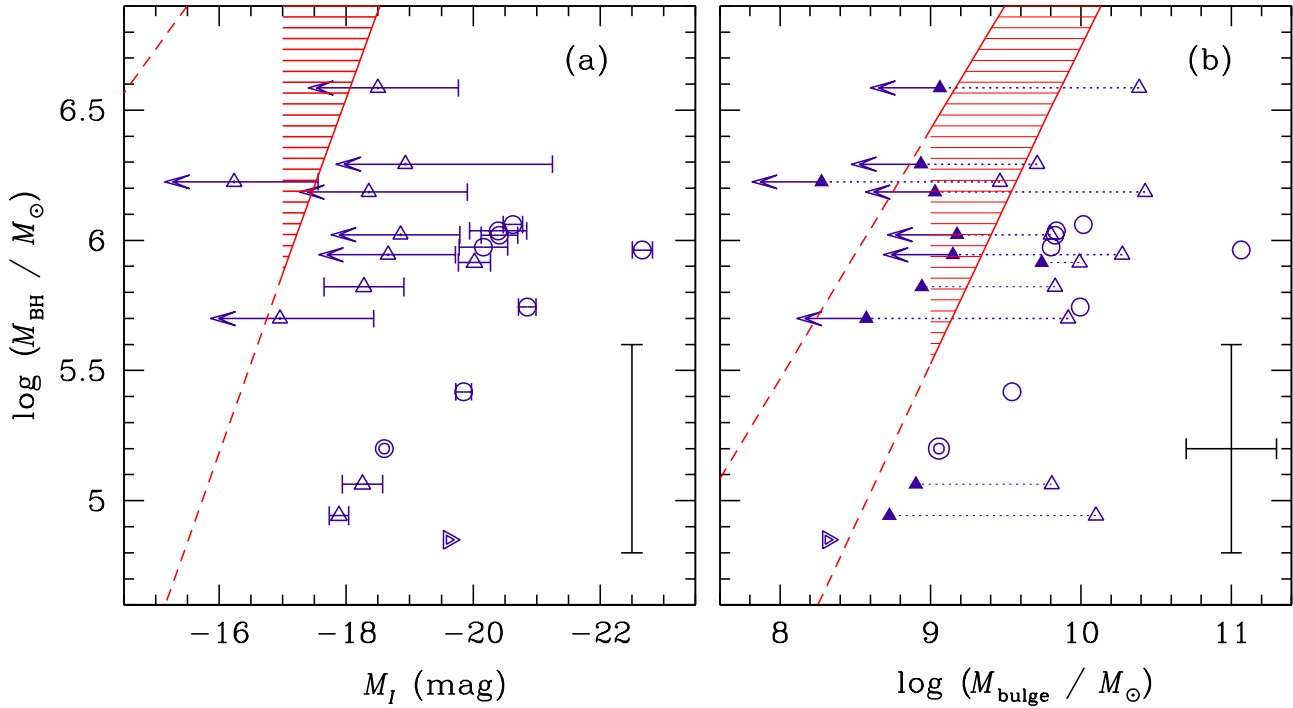


FIG. 7.— (a)  $M_{\text{BH}}$  as a function of bulge luminosity in the  $I$  band. Different host morphologies are noted with different symbols as in Fig. 2 above. Upper limits to bulge-like components are shown as left-pointing arrows. A 0.4 dex uncertainty on  $M_{\text{BH}}$  (Greene & Ho 2006b) is shown schematically in the lower right-hand corner. Also included are the well-studied low-mass BHs in POX 52 (double circle) and NGC 4395 (double triangle). The hatched region shows the fit from Tundo et al. (2007) to inactive BHs with dynamical mass estimates, shifted to  $I$  band assuming a color  $r' - I = 1.07$  mag for E/S0 galaxies from Fukugita et al. (1995). (b)  $M_{\text{BH}}$  as a function of bulge mass as estimated for a single stellar population from Bruzual & Charlot (2003; see text for details). Total masses are shown as open circles for blobs and open triangles for disks, while bulge masses alone (derived assuming a constant  $\Upsilon_I$ ) are filled triangles. The  $M_{\text{BH}}-M_{\text{bulge}}$  relation of Häring & Rix (2004) is shown as the shaded region. The blobs are offset from the expected relation by  $\sim 1$  dex, while the bulge components appear to be rather consistent with the relation at higher mass. Overall, we see that the scatter is much larger at low mass. Although the stellar masses are subject to a number of systematic uncertainties discussed in the text, for a wide range of reasonable assumptions the observed offset remains. The representative error in the stellar masses of 0.3 dex is due to systematic effects as discussed in Kannappan & Gawiser (2007), but note that in practice our stellar masses should be lower limits rather than true measurements.

served offset is due to young stellar populations rather than a true excess of mass, since the real correlation is presumably with bulge mass rather than luminosity (e.g., Häring & Rix 2004). The fiducial stellar population assumptions described above provide estimates of the host stellar masses (Fig. 7b). Again, we argue that the corrections are maximal since we have completely neglected an old (faint) stellar component. Therefore, these masses represent a lower limit on the true stellar mass. Even so, all of the detected bulges remain systematically offset from the relation toward higher stellar mass. Reassuringly, our masses agree remarkably well with the  $k$ -correct masses,  $\langle \log M_{\text{our}} - \log M_{k\text{cor}} \rangle = 0.02 \pm 0.06$ , which include a more sophisticated treatment of both the star formation history and the dust reddening. However, the treatment of stellar evolution and the adopted IMF are the same for the two methods, and systematic differences in these two assumptions dominate uncertainties in the mass estimates (e.g., Maraston 2005; Kannappan & Gawiser 2007). Nevertheless, the BH masses for the detected bulges and blobs are an order of magnitude lower than expected from the inactive  $M_{\text{BH}}-M_{\text{bulge}}$  relation, which is a large offset compared to the probable systematics. Taking the virial masses at face value, we find that the ratio of BH mass to bulge mass is considerably lower in these galaxies compared to their high-mass cousins. Interestingly, G1 (Gebhardt et al. 2002, 2005) and Omega Cen (Noyola et al. 2008) display the opposite trend (their ratios of BH mass to bulge mass are closer to  $10^2$  than to  $10^3$ ).

Finally, we recall that our sample as a whole is biased toward the host galaxies that are luminous enough to be targeted spectroscopically by the SDSS survey (Greene & Ho 2007b). We may simply have selected the luminous tail of the full dis-

tribution, and we do see that the bulges of the disk galaxies fall closer to the inactive relation than do the blobs (Fig. 7b). While we cannot quantify the true distribution of host galaxy mass at a given  $M_{\text{BH}}$ , we can rule out that these galaxies are drawn from the same distribution as the inactive sample. There is a 1 mag scatter ( $1 \sigma$ ) about a fixed BH mass in the inactive sample (where we have used the best-fit line of Tundo et al. 2007 and the data compiled in Häring & Rix 2004). At the median  $M_{\text{BH}}$  of the blobs ( $\sim 10^6 M_{\odot}$ ), the median host luminosity is  $M_I = -20.4$  mag, which is  $2.4 \sigma$  from the expected central value of  $M_I = -17.9$  mag. Thus, in order to be consistent with the observed central value and scatter for the inactive relation, we would require that the galaxy luminosity function rise by a factor of 300 between  $M_I = -18$  mag and  $M_I = -20$  mag, which can be ruled out categorically (e.g., Blanton et al. 2003b). Of course, we must implicitly assume that the active fraction is constant over this range. While AGN activity may depend on mass and Hubble type at some level, the dependence cannot change so radically. Furthermore, we have ignored the additional scatter introduced by the virial BH mass measurements, largely because that scatter is poorly quantified. However, if we adopt the 0.4 dex scatter measured in the  $M_{\text{BH}}-\sigma_*$  relation by Greene & Ho (2006b), the calculation is unchanged. Although we cannot measure the true distribution of galaxy luminosity around BH mass, we can robustly conclude that it is different in this regime. Finally, we cannot presently rule out that some combination of systematic errors in the BH masses, selection bias in the host population, and uncertainties in the host galaxy masses are conspiring to cause the observed offset. While we view the possibility of a large systematic offset in the BH masses of the blob galaxies as unlikely, only a reverbera-

tion mapping campaign for these galaxies can help to settle this potential caveat.

## 6. DISCUSSION

While the absence of a BH in M33 (Gebhardt et al. 2001) tells us that not all late-type galaxies contain BHs, this sample confirms unambiguously that galaxies without classical bulges may nevertheless contain nuclear BHs. We already knew of a few such systems. The prototype is the BH in the late-type spiral galaxy NGC 4395, but AGNs have been detected recently in two other late-type spiral galaxies, NGC 3621 (Satyapal et al. 2007) and NGC 1042 (Shields et al. 2008). There is also a BH in POX 52, which is probably a spheroidal (Barth et al. 2004; Thornton et al. 2008). The galaxies presented here, as a whole, span a wide range in morphological type, but in general are inconsistent with being classical bulges. Adopting reasonable assumptions about the stellar populations of the galaxies in this study, we find that the compact blobs deviate from the fundamental plane of ellipticals toward the locus of spheroidal galaxies. We argue that the disk galaxies are inconsistent with having classical bulges, although we do not have direct structural measurements in most cases. Interestingly, other samples of low-mass, highly accreting BHs are also found preferentially in late-type spiral galaxies with a high fraction of strong bars (e.g., Crenshaw et al. 2003, although see also Ohta et al. 2007) and nuclear dust spirals (Deo et al. 2006).

Apparently galaxies can form central BHs even when they do not form classical bulges, but the process that results in the  $M_{\text{BH}} - M_{\text{bulge}}$  relation in bulge-dominated systems may or may not operate in the low-mass regime. Recall that, unfortunately, observational constraints from dynamical BH masses are very sparse in this regime. There are no dynamical BH mass measurements in spheroidal galaxies (aside from the upper limit in NGC 205 [Valluri et al. 2005] and very loose upper limits for a handful of Virgo spheroidals [Geha et al. 2002]), and so a different  $M_{\text{BH}} - M_{\text{bulge}}$  relationship, or a significant increase in the scatter, cannot be ruled out for galaxies of this type. There are a handful of dynamical masses measured in pseudobulges, which may suggest that the BHs are in general undermassive compared to  $M_{\text{bulge}}$  (C. Y. Peng & L. C. Ho 2008, in preparation) or  $\sigma_*$  (Hu 2008). However, some of the masses are based on highly uncertain maser kinematics, and it may be premature to draw strong conclusions. It is clear that the  $M_{\text{BH}} - M_{\text{bulge}}$  relation breaks down at low mass, at least for this sample. We have only weak constraints on the relation between BH and pseudobulge mass, but the blob galaxies are clearly overly massive compared to their central BHs. Before we attempt to interpret this result in the context of the galaxy population as a whole, however, we must consider the possibility that our result is peculiar to actively accreting BHs.

The BHs in our sample are currently radiating and thus gaining mass. Many authors have suggested that vigorously accreting local BHs are growing toward the  $M_{\text{BH}} - \sigma_*$  relation, based on estimates for  $\sigma_*$  from narrow emission-line widths (typically the [O III]  $\lambda 5007$  line; e.g., Grupe & Mathur 2004; Bian & Zhao 2004). On the other hand, the reliability of the [O III] linewidth, which often displays a strongly asymmetric profile or is highly blueshifted, has been questioned (e.g., Boroson 2005; Greene & Ho 2005a), and indeed when lower-ionization lines are used instead, the deviations from the  $M_{\text{BH}} - \sigma_*$  relation appear to be

mitigated (e.g., Komossa & Xu 2007). Although it is observationally quite challenging to obtain direct  $\sigma_*$  measurements for BHs in a high accretion state in general, those galaxies for which it has been possible do not appear to deviate from the inactive  $M_{\text{BH}} - \sigma_*$  relation (Barth et al. 2005; Botte et al. 2005).

An interesting and independent constraint on the galaxy potential may be derived from circular velocity measurements. There is some suggestion that, at a given  $M_{\text{BH}}$ ,  $v_{\text{max}}$  as measured from H I is lower at high Eddington ratio, and the trend is significantly strengthened when one considers the galaxy dynamical mass (Ho et al. 2008). The sense is the same as the offset of  $\sim 0.17$  dex seen by Onken et al. (2004) and Greene & Ho (2006b) in the  $M_{\text{BH}} - \sigma_*$  relation of active galaxies. Furthermore, M. Kim et al. (in preparation) find that the most highly accreting local broad-line AGNs lie systematically below the  $M_{\text{BH}} - L_{\text{bulge}}$  relation. In all of these cases, however, the measured offset is closer to a factor of 2 in BH mass, consistent with a single Eddington-limited growth phase over a Salpeter time. The order-of-magnitude offset that we see here is much harder to reconcile with the inactive relationship. It seems more likely that the  $M_{\text{BH}} - M_{\text{bulge}}$  relation is simply different in this regime.

As an aside, we also note that the apparent evolution in the  $M_{\text{BH}} - M_{\text{bulge}}$  relation at high redshift is in the opposite sense to that observed here. At redshifts ranging from  $0.37 < z < 6.4$  numerous authors have found evidence for evolution in BH-host scaling relations, but the ratio of BH to bulge mass appears to increase at earlier times (e.g., Peng et al. 2006a,b; Woo et al. 2006; Shields et al. 2006; Salvander et al. 2006; Ho 2007). If we were seeing the impact of continuing evolution in  $M_{\text{BH}} - M_{\text{bulge}}$ , then we must either discount all of the above studies (although see Lauer et al. 2007b) or once again posit that mechanisms relating BH mass and galaxy mass are different for low-mass systems. Even if the  $M_{\text{BH}} - M_{\text{bulge}}$  relation continues to evolve to a small extent in low-mass active systems at low redshift, our data suggest that the final relation looks different at low mass.

Given that low-mass galaxies have different, presumably more quiescent, formation histories, a different relationship with their central BHs is not necessarily surprising. In fact, the BHs are of low enough mass that they are consistent with forming by a variety of seed production mechanisms (e.g., Portegies Zwart & McMillan 2002; Koushiappas et al. 2004; Begelman et al. 2006) and then growing minimally ever since. Perhaps in the absence of the violent, gas-rich events thought to be responsible for the formation of elliptical galaxies and classical bulges, BHs do not necessarily grow significantly. We have no direct constraints on the growth history of low-mass BHs from existing observations of the active BH mass function, which unfortunately are not constraining at low BH mass and high redshift (e.g., Heckman et al. 2004; Kollmeier et al. 2006; Greene & Ho 2007b; Shen et al. 2008b). If BH growth at low mass is driven by more stochastic processes (e.g., Hopkins & Hernquist 2006), then we might indeed expect to see a bias toward more massive host galaxies at a given BH mass.

On the other hand, while the  $M_{\text{BH}} - M_{\text{bulge}}$  relation appears to change with mass, we do have some evidence for continuity in the  $M_{\text{BH}} - \sigma_*$  relation for these systems (Barth et al. 2005). Given that the galaxies do not obey the fundamental plane of elliptical galaxies and classical bulges, we would not expect

<sup>8</sup>Barth et al. (2005) and Greene & Ho (2006b) both note the apparent flattening at low mass in the  $M_{\text{BH}} - \sigma_*$  relation slope. Even adopting the maximum contamination of 20% to  $\sigma_*$ , then, the ensemble would still be consistent with the  $M_{\text{BH}} - \sigma_*$  relation. Note that the data presented in Barth et al. (2005) have been used to support possible non-linearity in the  $M_{\text{BH}} - \sigma_*$  relation (e.g., Wyithe 2006). It is our opinion that, given the outstanding uncertainties in both the BH mass scale and

them to simultaneously obey  $M_{\text{BH}} - \sigma_*$  and  $M_{\text{BH}} - M_{\text{bulge}}$ . However, they could have easily obeyed neither<sup>8</sup>. Better statistics are needed, particularly since a fraction of our measurements are probably dominated by rotation, but it is at least intriguing that the  $M_{\text{BH}} - \sigma_*$  relation seems to be preserved, even for the massive globular clusters G1 and Omega Cen (Gebhardt et al. 2002, 2005; Noyola et al. 2008).

Are there any proposed mechanisms for establishing BH-bulge relations that specifically preserve an  $M_{\text{BH}} - \sigma_*$  relation but not necessarily  $M_{\text{BH}} - M_{\text{bulge}}$ ? Explanations for the  $M_{\text{BH}} - \sigma_*$  or  $M_{\text{BH}} - M_{\text{bulge}}$  relation that rely on BH self-regulation by construction do not predict any mass or structural dependence in the final relation. The BH grows until it is massive enough to unbind the gas in the galaxy (e.g., Silk & Rees 1998; Murray et al. 2005). One alternative is suggested by Peng (2007), who proposes that merging in a hierarchical universe, combined with a mass function that rises toward low mass, will lead to a tight correlation between BH mass and bulge mass at the luminous end. In this scenario the BH-galaxy relations at low mass begin to depend in detail on the merger histories of the galaxies, and it is not clear that an  $M_{\text{BH}} - \sigma_*$  relation would necessarily result. Perhaps the most promising alternative is that BH growth really depends on a (relatively) local stellar velocity dispersion, as would be expected for instance in a model where the accretion disk is fed by the capture of individual stars (Miralda-Escudé & Kollmeier 2005).

We should note that there are other regimes in which the  $M_{\text{BH}} - \sigma_*$  and  $M_{\text{BH}} - M_{\text{bulge}}$  relations cannot be simultaneously valid. The most luminous elliptical galaxies, particularly brightest cluster galaxies, also deviate from the fundamental plane of regular ellipticals and classical bulges; while  $\sigma_*$  saturates at  $\sim 400 \text{ km s}^{-1}$  (and correspondingly  $M_{\text{BH}} \approx 3 \times 10^9 M_{\odot}$ ), the luminosities and effective radii of brightest cluster galaxies continue to rise (e.g., Bernardi et al. 2007; Lauer et al. 2007a). Although it is difficult to obtain dynamical BH masses for brightest cluster galaxies outside of the Virgo Cluster, Lauer et al. argue that in this regime bulge luminosity may be a better predictor of  $M_{\text{BH}}$  than is  $\sigma_*$ . Massive elliptical galaxies are characterized by a deficit of light in their inner profiles, perhaps because the innermost stars have been ejected through three-body interactions with a binary BH (e.g., Faber et al. 1997). Within this framework, the size of the core serves as an indirect probe of  $M_{\text{BH}}$ . Since core size correlates more strongly with bulge luminosity than with  $\sigma_*$ , Lauer et al. (2007a) propose that bulge luminosity is a better predictor of BH mass. More dynamical BH masses are needed, at both mass extremes, to settle this question.

In short, it is clear that the relationship between BH mass and “bulge” mass changes in low-mass systems without classical bulges. It is implausible that the BHs will grow sufficiently to lie on the  $M_{\text{BH}} - M_{\text{bulge}}$  relation. Given the different formation histories of the low-mass galaxies compared to classical bulges and elliptical galaxies, it seems more likely that the  $M_{\text{BH}} - M_{\text{bulge}}$  relation just changes in this regime. In contrast, the  $M_{\text{BH}} - \sigma_*$  relation appears to continue to low mass with less scatter than the  $M_{\text{BH}} - M_{\text{bulge}}$  relation. It will be interesting to see whether these trends persist with larger and less biased samples.

## 7. SUMMARY

the contributions of rotation to some objects, these claims are rather premature.

We have used *HST*-ACS images, in combination with  $\sigma_*$  measurements, to examine the host galaxy structures for a sample of low-mass active galaxies. The systems in this study were selected based on BH mass rather than galaxy properties, in order to investigate the range of host structures and luminosities that host low-mass BHs. We find that the host galaxies are relatively faint; with  $\langle M_I \rangle = -20.7$  mag, they are  $\sim 1$  mag below  $L^*$  at  $z = 0.1$ . The colors are typical of Sa galaxies,  $\langle B - I \rangle = 2.0 \pm 0.2$  mag. There are 11 disk galaxies (although two of those have ambiguous classifications) and 7 compact blobs with no evidence of a disk component. All of the disk galaxies are consistent with containing a bulge, but in seven of the 11 disks we can only place limits on the bulge luminosities.

The structural measurements from the ACS images, combined with  $\sigma_*$  measurements from Barth et al. (2005), allow an investigation of the fundamental plane locations for the bulge-like components of the galaxies. We find that once stellar population and reddening effects are accounted for, the compact blobs are closer to the locus of spheroidal galaxies than that of elliptical galaxies or classical bulges. We argue that the disk galaxies probably all contain pseudobulges, although we detect them in only a handful of cases. Our result provides strong confirmation that BHs are found even in the absence of classical bulges. At the same time, the ratio of BH to bulge mass in these systems is considerably lower than in more massive inactive systems. Perhaps, therefore, the process that builds bulges is required to stimulate healthy BH growth. Alternatively, it may be that the BH is more sensitive to the central stellar velocity dispersion than to the details of galaxy formation.

Some immediate progress will be made in clarifying the trends we observe. We are currently in the process of collecting comparable data for nearly an order of magnitude more objects (Greene & Ho 2007c). Hopefully it will be possible to obtain reverberation mapping masses for low-mass systems in addition to NGC 4395 (Peterson et al. 2005). Optical monitoring campaigns, to identify suitable candidates, are underway. Both of these endeavors will provide a clearer picture of the relation between BH mass and galaxy properties at low mass. Meanwhile, alternate search techniques (e.g., Satyapal et al. 2007; Ulvestad et al. 2007; Desroches & Ho 2008) may help to mitigate the biases in host galaxy properties suffered by this optically selected sample. At the same time, an increased sample of dynamical BH masses in spiral galaxies would be extremely useful in elucidating the true BH-galaxy relations at low mass.

We thank J. Kormendy both for many useful conversations, and for providing the fundamental plane data prior to publication. It would not be possible to thank C. Y. Peng adequately, not only for developing and supporting GALFIT, but also for answering countless technical questions that arose during the course of this research, and for stimulating science discussions as well. We thank P. Martini for providing the cosmic ray removal software, K. Gebhardt for helpful suggestions and A. Socrates for interesting discussions. Finally, we acknowledge the anonymous referee for a very careful reading of the manuscript and comments that significantly improved this paper. Support for J. E. G. was provided by NASA through Hubble Fellowship grant HF-01196, and support for L. C. H. was provided by HST-GO-10586.01-A, both awarded by the Space Telescope Science Institute, which is operated by the Association of Universities for Research in Astronomy, Inc., for NASA,

under contract NAS 5-26555. Research by A. J. B. is supported by the National Science Foundation under Grant No. AST-0548198. Funding for the SDSS has been provided by the Alfred P. Sloan Foundation, the Participating Institutions, the National Science Foundation, the U.S. Department of Energy, the National Aeronautics and Space Administration, the

Japanese Monbukagakusho, the Max Planck Society, and the Higher Education Funding Council for England. The SDSS web site is <http://www.sdss.org/>. This research has made use of data obtained from the High Energy Astrophysics Science Archive Research Center (HEASARC), provided by NASA's Goddard Space Flight Center.

## APPENDIX

### NOTES ON INDIVIDUAL GALAXIES

#### *GH04*

In the *I* band GH04 is a compact bulge-like system. Structurally it sits on the fundamental plane, although it is significantly offset in the Faber-Jackson relation. The most interesting aspect of this system is the “tail” most easily seen in the *B*-band image (Fig. A8), extending to the East of the nucleus. Given that we have strong upper limits on the radio emission from GH04 (Greene et al. 2006), this feature is more likely associated with the accretion of a small satellite or star formation in the host galaxy than some sort of jet feature.

#### *GH07*

GH07 is one of the three clear spheroidals in the sample. It is unremarkable in terms of luminosity and color, but is one of the most asymmetric objects in the sample. The residuals from the GALFIT in Figure 1 show this asymmetry most clearly. There is a clear excess above the symmetric model to the North-West. There is also a faint galaxy in the field to the North.

#### *GH09*

GH09 is the most luminous and the reddest galaxy in our sample. It very clearly lies on the fundamental plane of ellipticals and classical bulges (although we do not have a stellar velocity dispersion measurement for it). In terms of the properties of the objects in our sample, this galaxy is a clear outlier. It would be very interesting if this massive galaxy actually hosts a  $10^6 M_\odot$  BH, but in this case the more likely scenario seems to be that we have seriously underestimated the BH mass. We could benefit from a higher signal-to-noise ratio spectrum at higher resolution to perform an improved fit to the linewidth, but it would also be desirable to obtain reverberation mapping for this source, to see if it really is such a deviant system.

#### *GH11*

This galaxy has the dubious distinction of being the most difficult to model. Although it is very compact, it appears to have a distinct shelf of emission in the inner few arcseconds (Figs. 1, A8). In Figure A5 we show the blue image of GH11, in which an asymmetric ring is very evident. It appears that the galaxy has an asymmetric ring of star formation with a the radius is  $0''.3$ , or  $\sim 500$  pc away from the nucleus, which is consistent with the sizes of nuclear rings in mid-type spiral galaxies (e.g., Buta & Combes 1996). In support of the idea that this ring of excess emission is actively forming stars is the fact that GH11 is the bluest galaxy in our sample, and also (interestingly) has the largest [O II]/[O III] ratio in the sample. Ho (2005; see also Kim et al. 2006) suggests that the [O II]/[O III] may be a good indicator of ongoing star formation activity in AGNs, since [O II] is intrinsically weak in high-ionization Seyfert galaxies.

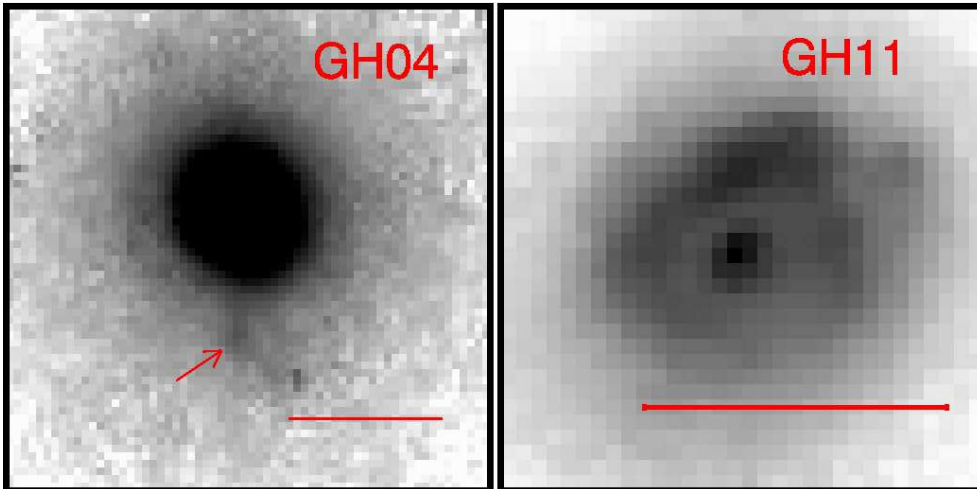


FIG. A8.— *B*-band images for GH04 and GH11. Scale bars are  $1''$  in length. Note the tail in GH04 and the blue knot or ring in GH11.

## REFERENCES

- Alongi, M., Bertelli, G., Bressan, A., Chiosi, C., Fagotto, F., Greggio, L., & Nasi, E. 1993, *A&AS*, 97, 851
- Andredakis, Y. C., Peletier, R. F., & Balcells, M. 1995, *MNRAS*, 275, 874
- Barth, A. J., Greene, J. E., & Ho, L. C. 2005, *ApJ*, 619, L151
- Barth, A. J., Ho, L. C., Rutledge, R. E., & Sargent, W. L. W. 2004, *ApJ*, 607, 90
- Begelman, M. C., Volonteri, M., & Rees, M. J. 2006, *MNRAS*, 370, 289
- Bell, E. F., et al. 2006, *ApJ*, 640, 241
- Bender, R., Burstein, D., & Faber, S. M. 1992, *ApJ*, 399, 462
- Bentz, M. C., Peterson, B. M., Pogge, R. W., Vestergaard, M., & Onken, C. A. 2006, *ApJ*, 644, 133
- Bernardi, M., et al. 2003, *AJ*, 125, 1849
- Bernardi, M., Hyde, J. B., Sheth, R. K., Miller, C. J., & Nichol, R. C. 2007, *AJ*, 133, 1741
- Bian, W., & Zhao, Y. 2004, *MNRAS*, 352, 823
- Blandford, R. D., & McKee, C. F. 1982, *ApJ*, 255, 419
- Blanton, M. R., et al. 2003a, *AJ*, 125, 2348
- . 2003b, *ApJ*, 592, 819
- Blanton, M. R., & Roweis, S. 2007, *AJ*, 133, 734
- Böker, T., Laine, S., van der Marel, R. P., Sarzi, M., Rix, H.-W., Ho, L. C., & Shields, J. C. 2002, *AJ*, 123, 1389
- Boroson, T. A. 2005, *AJ*, 130, 381
- Botte, V., Ciroti, S., di Mille, F., Rafanelli, P., & Romano, A. 2005, *MNRAS*, 356, 789
- Bottema, R. 1993, *A&A*, 275, 16
- Bressan, A., Fagotto, F., Bertelli, G., & Chiosi, C. 1993, *A&AS*, 100, 647
- Bruzual, G., & Charlot, S. 2003, *MNRAS*, 344, 1000
- Burstein, D., Bender, R., Faber, S., & Nolthenius, R. 1997, *AJ*, 114, 1365
- Buta, R., & Combes, F. 1996, *Fundamentals of Cosmic Physics*, 17, 95
- Byun, Y. I., & Freeman, K. C. 1995, *ApJ*, 448, 563
- Caon, N., Capaccioli, M., & D'Onofrio, M. 1993, *MNRAS*, 265, 1013
- Cappellari, M., et al. 2006, *MNRAS*, 366, 1126
- Cardelli, J. A., Clayton, G. C., & Mathis, J. S. 1989, *ApJ*, 345, 245
- Carollo, C. M. 1999, *ApJ*, 523, 566
- Carollo, C. M., Stiavelli, M., Seigar, M., de Zeeuw, P. T., & Dejonghe, H. 2002, *AJ*, 123, 159
- Chabrier, G. 2003, *ApJ*, 586, L133
- Ciotti, L., & Bertin, G. 1999, *A&A*, 352, 447
- Collin, S., Kawaguchi, T., Peterson, B. M., & Vestergaard, M. 2006, *A&A*, 456, 75
- Côté, P., et al. 2006, *ApJS*, 165, 57
- Courteau, S., de Jong, R. S., & Broeils, A. H. 1996, *ApJ*, 457, L73
- Crenshaw, D. M., Kraemer, S. B., & Gabel, J. R. 2003, *AJ*, 126, 1690
- de Jong, R. S. 1996a, *A&AS*, 118, 557
- . 1996b, *A&A*, 313, 45
- Deo, R. P., Crenshaw, D. M., & Kraemer, S. B. 2006, *AJ*, 132, 321
- De Rijcke, S., Dejonghe, H., Zeilinger, W. W., & Hau, G. K. T. 2004, *A&A*, 426, 53
- De Rijcke, S., Prugniel, P., Simien, F., & Dejonghe, H. 2006, *MNRAS*, 369, 1321
- Desroches, L.-B., & Ho, L. C. 2008, *ApJ*, submitted
- de Vaucouleurs, G. 1948, *Annales d'Astrophysique*, 11, 247
- Djorgovski, S., & Davis, M. 1987, *ApJ*, 313, 59
- Dressler, A., Lynden-Bell, D., Burstein, D., Davies, R. L., Faber, S. M., Terlevich, R., & Wegner, G. 1987, *ApJ*, 313, 42
- Faber, S. M., et al. 1997, *AJ*, 114, 1771
- Faber, S. M., & Jackson, R. E. 1976, *ApJ*, 204, 668
- Fagotto, F., Bressan, A., Bertelli, G., & Chiosi, C. 1994a, *A&AS*, 104, 365
- . 1994b, *A&AS*, 105, 29
- Ferrarese, L., et al. 2006, *ApJS*, 164, 334
- Ferrarese, L., Pogge, R. W., Peterson, B. M., Merritt, D., Wandel, A., & Joseph, C. L. 2001, *ApJ*, 555, L79
- Filippenko, A. V., & Ho, L. C. 2003, *ApJ*, 588, L13
- Filippenko, A. V., & Sargent, W. L. W. 1988, *ApJ*, 324, 134
- Freeman, K. C. 1966, *MNRAS*, 133, 47
- Fruchter, A. S., & Hook, R. N. 2002, *PASP*, 114, 144
- Fukugita, M., Shimasaku, K., & Ichikawa, T. 1995, *PASP*, 107, 945
- Gavazzi, G., Donati, A., Cucciati, O., Sabatini, S., Boselli, A., Davies, J., & Zibetti, S. 2005, *A&A*, 430, 411
- Gebhardt, K., et al. 2000a, *ApJ*, 539, L13
- . 2000b, *ApJ*, 543, L5
- . 2001, *AJ*, 122, 2469
- Gebhardt, K., Rich, R. M., & Ho, L. C. 2002, *ApJ*, 578, L41
- . 2005, *ApJ*, 634, 1093
- Geha, M., Guhathakurta, P., & van der Marel, R. P. 2002, *AJ*, 124, 3073
- Girardi, L., Bressan, A., Chiosi, C., Bertelli, G., & Nasi, E. 1996, *A&AS*, 117, 113
- Graham, A. W., & Guzmán, R. 2003, *AJ*, 125, 2936
- Graham, A., Lauer, T. R., Colless, M., & Postman, M. 1996, *ApJ*, 465, 534
- Greene, J. E., & Ho, L. C. 2004, *ApJ*, 610, 722
- . 2005a, *ApJ*, 627, 721
- . 2005b, *ApJ*, 630, 122
- . 2006a, *ApJ*, 641, 114
- . 2006b, *ApJ*, 641, L21
- . 2007a, *ApJ*, 656, 84
- . 2007b, *ApJ*, 667, 131
- . 2007c, *ApJ*, 670, 92
- Greene, J. E., Ho, L. C., & Ulvestad, J. S. 2006, *ApJ*, 636, 56
- Grupe, D., & Mathur, S. 2004, *ApJ*, 606, L41
- Häring, N., & Rix, H.-W. 2004, *ApJ*, 604, L89
- Heckman, T. M., Kauffmann, G., Brinchmann, J., Charlot, S., Tremonti, C., & White, S. D. M. 2004, *ApJ*, 613, 109
- Ho, L. C. 2005, *ApJ*, 629, 680
- . 2007, *ApJ*, 669, 821
- Ho, L. C., Darling, J., & Greene, J. E. 2008, *ApJ*, in press (astroph/0803.1952)
- Ho, L. C., & Peng, C. Y. 2001, *ApJ*, 555, 650
- Hopkins, P. F., & Hernquist, L. 2006, *ApJS*, 166, 1
- Hopkins, P. F., Hernquist, L., Cox, T. J., Di Matteo, T., Robertson, B., & Springel, V. 2006, *ApJS*, 163, 1
- Hu, J. 2008, *MNRAS*, submitted (astroph/0801.1481)
- Jahnke, K., et al. 2004, *ApJ*, 614, 568
- Jedrzejewski, R. I. 1987, *MNRAS*, 226, 747
- Jerjen, H., & Binggeli, B. 1997, in *The Second Stromlo symposium: The Nature of Elliptical Galaxies*, ed. M. Arnaboldi et al. (San Francisco: ASP), 239
- Jørgensen, I., Franx, M., & Kjaergaard, P. 1995, *MNRAS*, 276, 1341
- Kannappan, S. J., & Gawiser, E. 2007, *ApJ*, 657, L5
- Kaspi, S., Maoz, D., Netzer, H., Peterson, B. M., Vestergaard, M., & Jannuzi, B. T. 2005, *ApJ*, 629, 61
- Kim, M., Ho, L. C., & Im, M. 2006, *ApJ*, 642, 702
- Kim, M., Ho, L. C., Peng, C. Y., & Im, M. 2007, *ApJ*, 658, 107
- Koekemoer, A. M., Fruchter, A. S., Hook, R. N., & Hack, W. 2002, in *The 2002 HST Calibration Workshop*, ed. S. Arribas, A. Koekemoer, & B. Whitmore. (Baltimore, MD: STScI), 337
- Kollmeier, J. A., et al. 2006, *ApJ*, 648, 128
- Komossa, S., & Xu, D. 2007, *ApJ*, 667, L33
- Kormendy, J. 1977, *ApJ*, 218, 333
- . 1985, *ApJ*, 295, 73
- Kormendy, J., & Djorgovski, S. 1989, *ARA&A*, 27, 235
- Kormendy, J., Fisher, D. B., Cornell, M. E., & Bender, R. 2008, *ApJ*, submitted
- Kormendy, J., & Kennicutt, R. C. 2004, *ARA&A*, 42, 603
- Koushiappas, S. M., Bullock, J. S., & Dekel, A. 2004, *MNRAS*, 354, 292
- Krist, J. 1995, in *ASP Conf. Ser. 77, Astronomical Data Analysis Software and Systems IV*, ed. R. A. Shaw, H. E. Payne, & J. J. E. Hayes (San Francisco: ASP), 349
- Krolik, J. H. 2001, *ApJ*, 551, 72
- Kunth, D., Sargent, W. L. W., & Bothun, G. D. 1987, *AJ*, 93, 29
- Lauer, T. R., et al. 2007a, *ApJ*, 662, 808
- Lauer, T. R., Tremaine, S., Richstone, D., & Faber, S. M. 2007b, *ApJ*, 670, 249
- MacArthur, L. A., Courteau, S., & Holtzman, J. A. 2003, *ApJ*, 582, 689
- Maraston, C. 2005, *MNRAS*, 362, 799
- Mateo, M. L. 1998, *ARA&A*, 36, 435
- Matković, A., & Guzmán, R. 2005, *MNRAS*, 362, 289
- McConnachie, A. W., & Irwin, M. J. 2006, *MNRAS*, 365, 1263
- Merritt, D., Milosavljević, M., Favata, M., Hughes, S. A., & Holz, D. E. 2004, *ApJ*, 607, L9
- Miniutti, G., Ponti, G., Greene, J. E., Ho, L. C., Fabian, A. C., & Iwasawa, K. 2008, *MNRAS*, submitted
- Miralda-Escudé, J., & Kollmeier, J. A. 2005, *ApJ*, 619, 30
- Murray, N., Quataert, E., & Thompson, T. A. 2005, *ApJ*, 618, 569
- Nelson, C. H., Green, R. F., Bower, G., Gebhardt, K., & Weistrop, D. 2004, *ApJ*, 615, 652
- Noyola, E., Gebhardt, K., & Bergmann, M. 2008, *ApJ*, 676, 1008
- O'Donnell, J. E. 1994, *ApJ*, 422, 158
- Ohta, K., Aoki, K., Kawaguchi, T., & Kiuchi, G. 2007, *ApJS*, 169, 1
- Onken, C. A., Ferrarese, L., Merritt, D., Peterson, B. M., Pogge, R. W., Vestergaard, M., & Wandel, A. 2004, *ApJ*, 615, 645
- Pavlovsky, C., et al. 2005, *ACS Data Handbook, Version 4.0* (Baltimore: STScI)
- Peng, C. Y. 2002, *AJ*, 124, 294
- . 2007, *ApJ*, 671, 1098
- Peng, C. Y., Ho, L. C., Impey, C. D., & Rix, H.-W. 2002, *AJ*, 124, 266
- Peng, C. Y., Impey, C. D., Ho, L. C., Barton, E. J., & Rix, H.-W. 2006a, *ApJ*, 640, 114
- Peng, C. Y., Impey, C. D., Rix, H.-W., Kochanek, C. S., Keeton, C. R., Falco, E. E., Lehar, J., & McLeod, B. A. 2006b, *ApJ*, 649, 616
- Peterson, B. M., et al. 2004, *ApJ*, 613, 682
- . 2005, *ApJ*, 632, 799
- Pizzella, A., Corsini, E. M., Dalla Bontà, E., Sarzi, M., Coccato, L., & Bertola, F. 2005, *ApJ*, 631, 785
- Portegies Zwart, S. F., & McMillan, S. L. W. 2002, *ApJ*, 576, 899
- Rhodes, J. D., et al. 2007, *ApJS*, 172, 203
- Rhodes, J. D., Massey, R., Albert, J., Taylor, J. E., Koekemoer, A. M., & Leauthaud, A. 2006, in *The 2005 HST Calibration Workshop*, ed. A. Koekemoer, P. Goudfroi, & L. Dressel. (Baltimore, MD: STScI), 21
- Robertson, B., Cox, T. J., Hernquist, L., Franx, M., Hopkins, P. F., Martini, P., & Springel, V. 2006, *ApJ*, 641, 21
- Salviander, S., Shields, G. A., Gebhardt, K., & Bonning, E. W. 2007, *ApJ*, 662, 131

- Satyapal, S., Vega, D., Heckman, T., O'Halloran, B., & Dudik, R. 2007, *ApJ*, 663, L9
- Schlegel, D. J., Finkbeiner, D. P., & Davis, M. 1998, *ApJ*, 500, 525
- Schombert, J. M. 1986, *ApJS*, 60, 603
- Sérsic, J. L. 1968, *Atlas de Galaxias Australes* (Córdoba: Obs. Astron., Univ. Nac. Córdoba)
- Shen, J., Vanden Berk, D. E., Schneider, D. P., & Hall, P. B. 2008a, *AJ*, 135, 928
- Shen, Y., Greene, J. E., Strauss, M., Richards, G. T., & Schneider, D. P. 2008b, *ApJ*, in press (astro-ph/0709.3098)
- Shields, G. A., Menezes, K. L., Massart, C. A., & Vanden Bout, P. 2006, *ApJ*, 641, 683
- Shields, J. C., Walcher, C. J., Böker, T., Ho, L. C., Rix, H.-W., & van der Marel, R. P. 2008, *ApJ*, accepted (astro-ph/0804.4024)
- Silk, J., & Rees, M. J. 1998, *A&A*, 331, L1
- Sirianni, M., et al. 2005, *PASP*, 117, 1049
- Spergel, D. N., et al. 2003, *ApJS*, 148, 175
- Thomas, D., Maraston, C., Bender, R., & Mendes de Oliveira, C. 2005, *ApJ*, 621, 673
- Thornton, C. E., Barth, A. J., Ho, L. C., Rutledge, R. E., & Greene, J. E. 2008, *ApJ*, submitted
- Tinsley, B. M. 1978, *ApJ*, 222, 14
- Tremaine, S., et al. 2002, *ApJ*, 574, 740
- Tundo, E., Bernardi, M., Hyde, J. B., Sheth, R. K., & Pizzella, A. 2007, *ApJ*, 663, 53
- Ulvestad, J. S., Greene, J. E., & Ho, L. C. 2007, *ApJ*, 661, L151
- Valluri, M., Ferrarese, L., Merritt, D., & Joseph, C. L. 2005, *ApJ*, 628, 137
- van Zee, L., Skillman, E. D., & Haynes, M. P. 2004, *AJ*, 128, 121
- Volonteri, M. 2007, *ApJ*, 663, L5
- Wadadekar, Y., Robbason, B., & Kembhavi, A. 1999, *AJ*, 117, 1219
- Wirth, A., & Gallagher, J. S., III 1984, *ApJ*, 282, 85
- Woo, J.-H., Treu, T., Malkan, M. A., & Blandford, R. D. 2006, *ApJ*, 645, 900
- Wyithe, J. S. B. 2006, *MNRAS*, 365, 1082
- York, D. G., et al. 2000, *AJ*, 120, 1579